UNITED NATIONS UNIVERSITY
UNU-GTP
Geothermal Training Programme

Orkustofnun, Grensasvegur 9,
IS-108 Reykjavik, Iceland

Reports 2019
Number 15

BOREHOLE GEOLOGY AND ALTERATION MINERALOGY OF WELL OW-205, OLKARIA GEOTHERMAL FIELD, KENYA

Christine N. Katana
Kenya Electricity Generating Company PLC – KenGen
P.O. Box 785 – 20117
Naivasha
KENYA
ckatana@kengen.co.ke, nyamvulachristine@gmail.com

ABSTRACT

Well OW-205 is an appraisal well drilled to open the Olkaria Central Field as well as to cater steam for the Olkaria VII power plant. Permeability in the well is controlled by the NW-SE fault in the west and the Ololbutot fault in the east. These faults facilitate near lateral movement of cold fluids in 1400-2000 m and are responsible for temperature reversals at this depth. Abundance of haematite, fluorite and sphene from 800 m to the bottom of the well (3000 m) has been associated with cooling. Possible processes proposed for causing the cooling conditions include mixing of brine and ca-rich meteoric fluids or mixing of two brines with different chemical composition. Temperature evolution around this area is associated with the NW-SE fault and the rejuvenated Ololbutot fault. In the area around well OW-205 two temperature regimes are found; relatively high paleo-temperatures of about 285°C and a lower temperature regime (225°C). With low temperatures around this well, it may not be suitable for production as it was planned initially. Alternative uses such as reinjection are an option since the well is intersecting with a deeper flow path of cooler fluids.

1. INTRODUCTION

The Olkaria geothermal field is a high-temperature field located within the Eastern branch of the East African Rift System (EARS). The EARS is 3000 km long and extends from the Afar triple junction in the north to Beira, Mozambique in the south. The rift is characterised by topographic uplifts of the Kenyan and Ethiopian dome, a series of graben basins joined by intracontinental transforms while segmented by accommodation and transfer zones. This rift system is a typical example of a divergent zone where spreading causes thinning of the crust and subsequent volcanism.

The EARS is divided into the Eastern and Western branches. The Kenyan rift lies in the Eastern branch where more intense tectono-volcanic activities are observed compared to the Western branch. Intense volcanism in this section led to the eruption of large shield volcanoes along the axis of the rift during the Quaternary. The Quaternary volcanoes in the central segment of the Kenyan rift include Barrier, Emuruangogolak, Silali, Paka and Korosi while those in the southern segment are Menengai, Eburru, Olkaria, Longonot and Suswa as shown in Figure 1. Most of these volcanoes have been explored for geothermal energy and are at different stages of exploration and development. The Olkaria volcanic

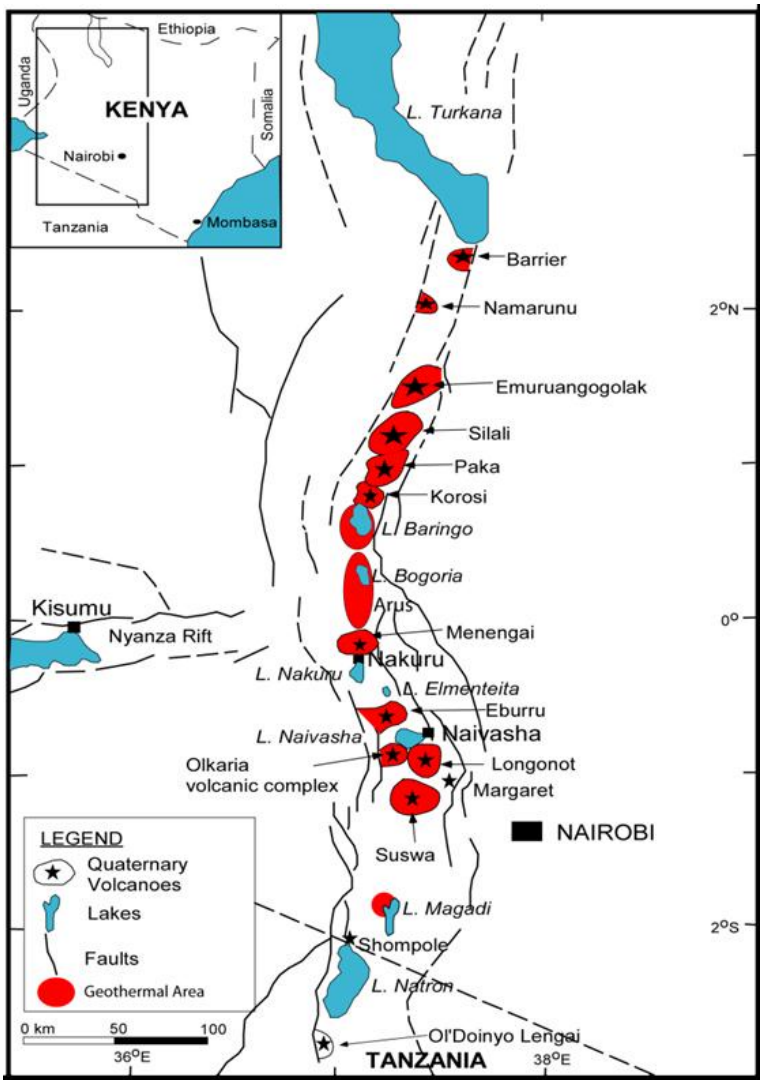

FIGURE 1: Map of the Kenyan rift system showing the location of potential geothermal prospects (Ofwona et al., 2006)

complex is the most explored among these and is in the advanced stages of development (Ofwona et al., 2006).

The Great Olkaria Volcanic Complex (GOVC) is located southwest of Lake Naivasha and west of the Longonot volcano and the resource area of the Olkaria geothermal field is estimated to be 204 km^2. Surface exploration in this field began in 1956 and the first exploration wells were drilled in 1970. Since then, wells have been drilled for different purposes including exploration, production, make up, step-out, re-injection etc. To date, the field has over 300 wells ranging from 500 to 3500 m in depth with an installed capacity of 683 MWe. Additional 150 MWe is expected by end of this year (2019) after the commissioning of the Olkaria V plant. For purposes of proper planning and development, the Olkaria geothermal field has been divided into seven sub-fields, namely Olkaria east, Olkaria northeast, Olkaria central, Olkaria northwest, Olkaria southeast, Olkaria southwest, and Olkaria domes, as outlined in Figure 2 with Olkaria Hill as reference point of the fields. A brief history of the exploration and development of the Olkaria field can be found in Saitet and Kwambai (2015).

This study focuses on well OW-205, along with wells OW-202 and OW-710. OW-205 is a vertical well located within the Olkaria Central Field at UTM coordinates E196609.3, N9903948.9 and 1903.86 m.a.s.l. It is an appraisal well that was drilled to open the Olkaria Central Field as well as to provide steam for the Olkaria VII geothermal power plant**.** The Central Field lies between the Olkaria northeast and Olkaria northwest field (Figure 3).

Exploration activities in the Olkaria Central Field began in the 1980s and by 1997, four wells had been drilled, namely OW-201, 202, 203 and 204. OW-201 and OW-204 are used for cold reinjection while OW-203 has been used for hot reinjection since 2003. OW-202 is the only productive well with a capacity of 1.4 MWe. It was drilled in 1996 but was not utilised until 2006 when it was leased to the Oserian Development Company (Opondo, 2015). OW-205 is the most recent well, it was drilled in 2016 and is yet to be utilised. Being the smallest and the least exploited compared the other fields, the Central Field hosts only a few wells thus borehole data is very scarce. This has motivated the study of OW-205. Findings from this study will be useful to update the Olkaria conceptual model, particularly in the central part of the field.

This research therefore seeks to understand the borehole geology of OW-205 through the analysis of drill cuttings, down-hole reservoir parameters and drilling parameters.
The specific objectives are:

- To identify subsurface geology of the well;
- To define hydrothermal alteration mineral assemblages;
- To understand thermal conditions and thermal history of the reservoir;
- To locate aquifers and permeable zones feeding the well.

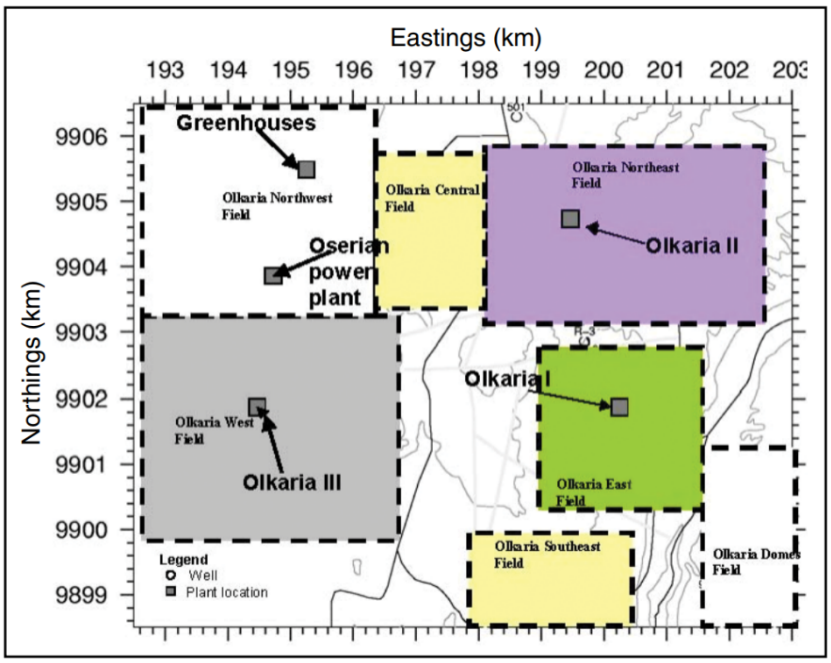

FIGURE 2: Production fields in the Olkaria geothermal field (modified from KenGen, 2017)

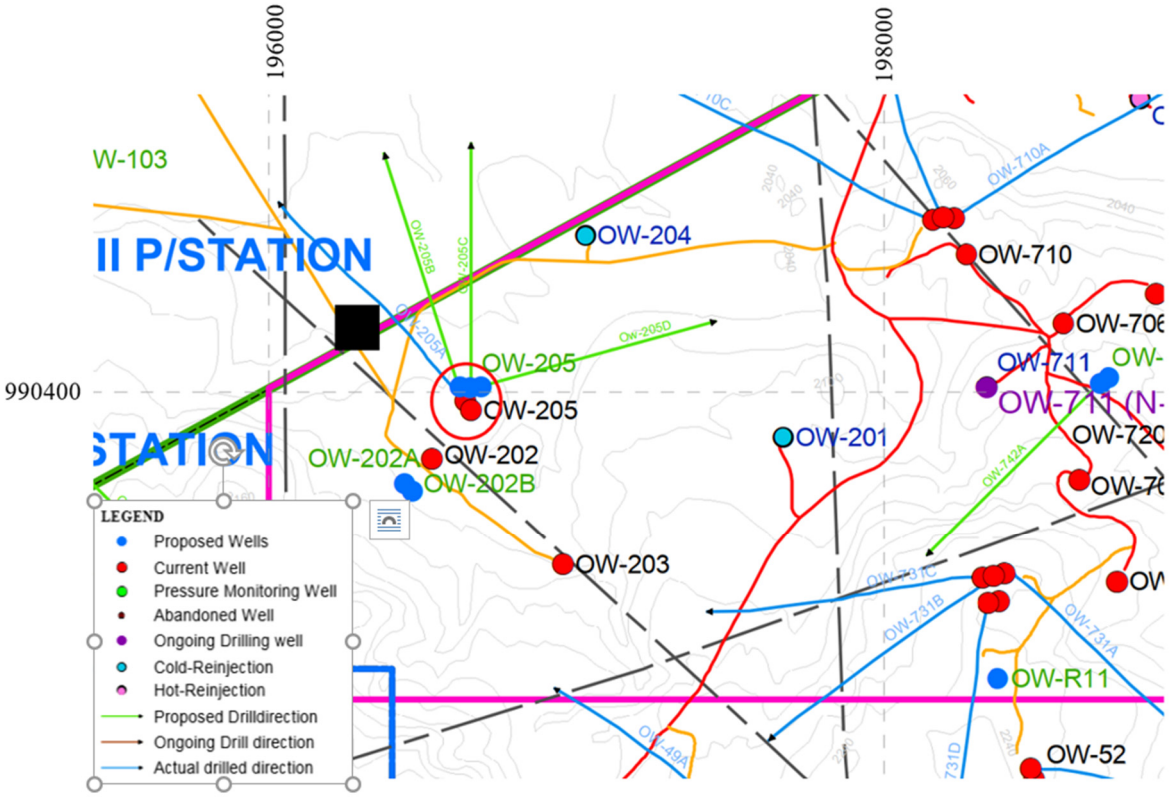

FIGURE 3: Location map for OW-205 (circled)

2. GEOLOGICAL AND STRUCTURAL SETTING OF THE OLKARIA GEOTHERMAL COMPLEX

2.1 Tectonic evolution and regional geology of East African Rift

The Olkaria volcanic complex is located within the southern segment of the Kenyan rift system, therefore its tectonic and geological evolution is related to that of the East African Rift. The East African Rift has been characterised by a series of graben valleys bounded by high continental shoulders with extensive normal faults and raised volcanic centres. Several studies have been conducted along the rift aimed at reconstructing the history of the basins and the rift shoulders as well as divulge the tectono-thermal phases related to the mantle plumes.

Pre-rifting volcanism started in the Turkana region (north Kenya) 45-37 Ma, resulting in the eruption of massive flood basalts and rhyolites while accompanied by extensive thermal uplift. Expansive volcanism dates to approximately 30 Ma in the Afar region. Eruption of trap lava flows was accompanied by the formation of three basin-like convergent structures, forming a triple junction (Chorowicz et al., 1998). At around 29-28 Ma, rifting had spread to the Gulf of Aden and by 27.5 Ma, rifting fracturing activities occurred south of the Red Sea (Hughes et al., 1991). Fracturing and subsidence propagated southward at different locations along the rift axis during the late Miocene. Episodes of volcanism continued in northern and central Kenya at 20 Ma and eventually propagated to the south towards North Tanzania in 5-8 Ma. Seismic activity indicates that the East African Rift is still active and propagates southwards at a mean rate of 2.5-5 cm/year (Hoffman et al., 1997, Kampunzu et al., 1998).

The Kenyan rift segment developed within the Neoprotezoic orogenic lithologies that include the Mozambique mobile belt of the Pan-African Orogeny (Fritz et al., 2013). Its rifting patterns and structure, volcanism and uplifting has been associated with the crustal configuration and weakness zones of the underlying Mozambique belt. Several theories have associated the origin of magma within the rift to tectono-magmatic activities influenced by mantle plumes, though the number of plumes is still debated (Macdonald, 2002). Upwelling of these plumes caused brittle fracturing of the crust into multiple normal faults. Prevailing magma fractionation within the lower crust and the upper mantle together with crustal assimilation led to the generation of greatly varied geology, ranging from alkaline to hyperalkaline volcanics with a wide range of isotopic and geochemical composition (Macdonald and Scaillet, 2006). For instance, the northern segment of the Kenyan rift is composed of theoleiitic and nepheline basalts while the central and southern segments are dominated by trachyte and pantellerites (Yirgu, 2009).

The early Miocene volcanism led to massive flood-basalts and phonolitic volcanism on the crest of an uplifting plume. This was followed by the graben forming event in the late Miocene that led to the eruption of large volumes of Pliocene ignimbrite-tuffs. Succeeding this event was the ignimbrite volcanism that resulted to the development of the major rift-bounding faults. Fissure eruptions of basalts and trachytes within the graben floor followed in the early Pleistocene. The formation of the graben and host features within the floor preceded the eruption of the Quaternary basalts, trachytes, phonolites, rhyolites and pyroclastics (Baker et al., 1972).

Macdonald and Scaillet (2006) has clearly demonstrated the complexity of the geology of the southern Kenyan rift, the youngest segment of the Kenyan rift system, is associated with Quaternary volcanism. This section encompasses five volcanic complexes, two of which are rhyolitic with no visible/clear caldera features (at Eburru and Olkaria) while the other areas (Menengai, Longonot and Suswa) are trachytic with distinct calderas. These complexes may be close to each other, but they have unique petrological characteristics. For instance, the Olkaria volcano is dominated by comendites, phonolites are only found in Suswa while Eburru is characterised by a combination of trachyte and pantellerite. Longonot and Menengai are mainly basalt-trachyte volcanoes (Clark et al, 1990). This has led to the conclusion that the comenditic rhyolites of the Eburru and Olkaria volcanoes were formed by crystal

fractionation of pantelleritic melts while the trachytic volcanoes were a result of fractionation of basaltic magma (Macdonald and Scaillet, 2006).

2.2 Geology and structural setting of the Great Olkaria Volcanic Complex (GOVC)

The Olkaria volcanic complex is a multicentred rhyolitic complex comprising of at least eighty small volcanic centres. Clark et al. (1990) associates its formation to a three-phased evolutionary process that begun with the pre-caldera activity which led to the eruption of trachyte-basalt lavas and pumice. This phase was followed by the fracture formation of the caldera and later eruption of welded pantellerites. The post-caldera activity in the third phase led to the formation of the Olkaria comenditic formations and later, the youngest Ololbutot comendite. These comendite members include the lower comendite member (>9150 BP), the middle comendite member (<9150,>3280 BP) and the upper comendite member (<3280 BP). The Ololbutot lava erupted along a north-south fissure in 180 ± 50 BP and Olkaria is still considered active to date (Macdonald and Scaillet, 2006).

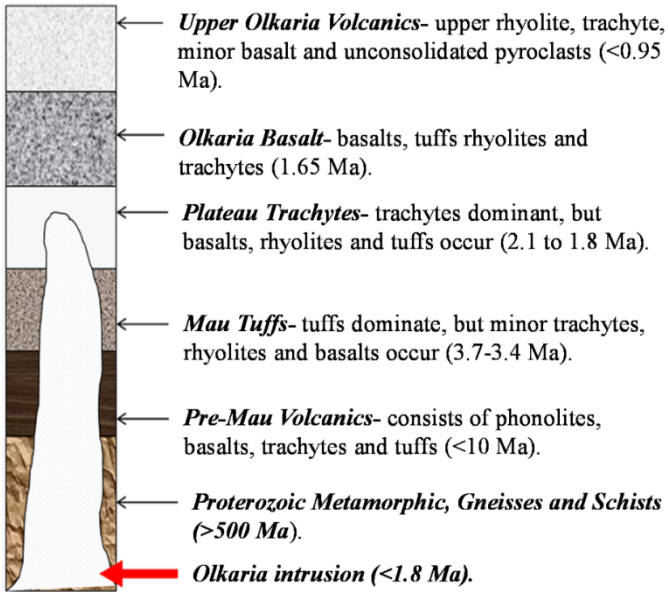

FIGURE 4: Stratigraphic column of the Olkaria volcanic complex (Omenda, 2000)

Surface and subsurface studies have indicated that the Olkaria Volcanic Complex has a wider lithological range from pyroclastics, ash, pumice and comendites on the surface to rhyolites, basalts, tuffs and trachytes in the subsurface (e.g. Omenda, 1998 and Marshall et al., 2009). The complexity of the geology and the overwhelming magma volumes have been attributed to the partial melting of the crustal rock, magma mixing and fractional crystallization (Macdonald, 2002). Analysis of borehole and surface data has led to lithological reconstruction of the entire complex which includes the 'basement' rocks of the Neoproterozoic, the pre-Mau volcanics, the Mau tuffs, the plateau trachytes and the Olkaria basalts and upper volcanics (Omenda, 1998, Omenda, 2000), as outlined in Figure 4.

The plateau lavas are composed of trachytic lavas with intercalations of rhyolite, tuff and basalt. The Olkaria basalts on the other hand comprise mainly of thin layers of basalts intercalated with thin layers of tuff, trachyte and rhyolites. The upper Olkaria volcanics constitute the surface rocks and represent the latest volcanic activities (Omenda, 1998).

As mentioned earlier, the Olkaria volcanic complex is situated on the floor of the southern segment of the Kenyan rift system and as such, all structures within it developed due to the characteristic weakness of the underlying crust. The topographic complexity has been associated with rifting and magmatism. Partial melting has led to the continuous eruption of large volumes of magma, a phenomenon that is regarded impossible by fractional crystallization (Bailey, 1974). Combined interpretation from geological and geophysical studies, satellite imagery, and aerial photography have revealed major structures within the Olkaria complex such as faults, fractures, dikes, domes/eruption centres, vents, plugs, sills and caldera as shown in Figure 5. Most of these structures are well exposed in the western part of the field and seem to be buried in the eastern part due to the thick Quaternary pyroclastic deposits in this area. Faults in the Olkaria volcanic complex have been classified into five sets according to their orientation. They include NW-SE, NNE-SSW, NE-SW, E-W and N-S orientations (Munyiri, 2016; Omenda, 1998).

The NW-SE faults are the oldest structures and characterise the basement of the rift. The Suswa fault and the Gorge Farm fault, located in the SW and NE corners, respectively, are good examples of these faults. The former intersects the NNE-SSW faults while the later controls both shallow and deep upflow zones. The NNE-SSW faults are regarded as old rejuvenated structures and they expose geothermal manifestations. The distinct one is the Ol Njorowa Gorge whose formation is associated with a cataclysmic flash flood that swept the area approximately 9000 years ago (Clarke et al., 1990). This structure has been useful for mapping the N-S trending dikes and plugs that are exposed within it. Another useful NNE-SSW fault is the Olkaria fault which is characterised by intense surface geothermal manifestations such as altered grounds and fumaroles.

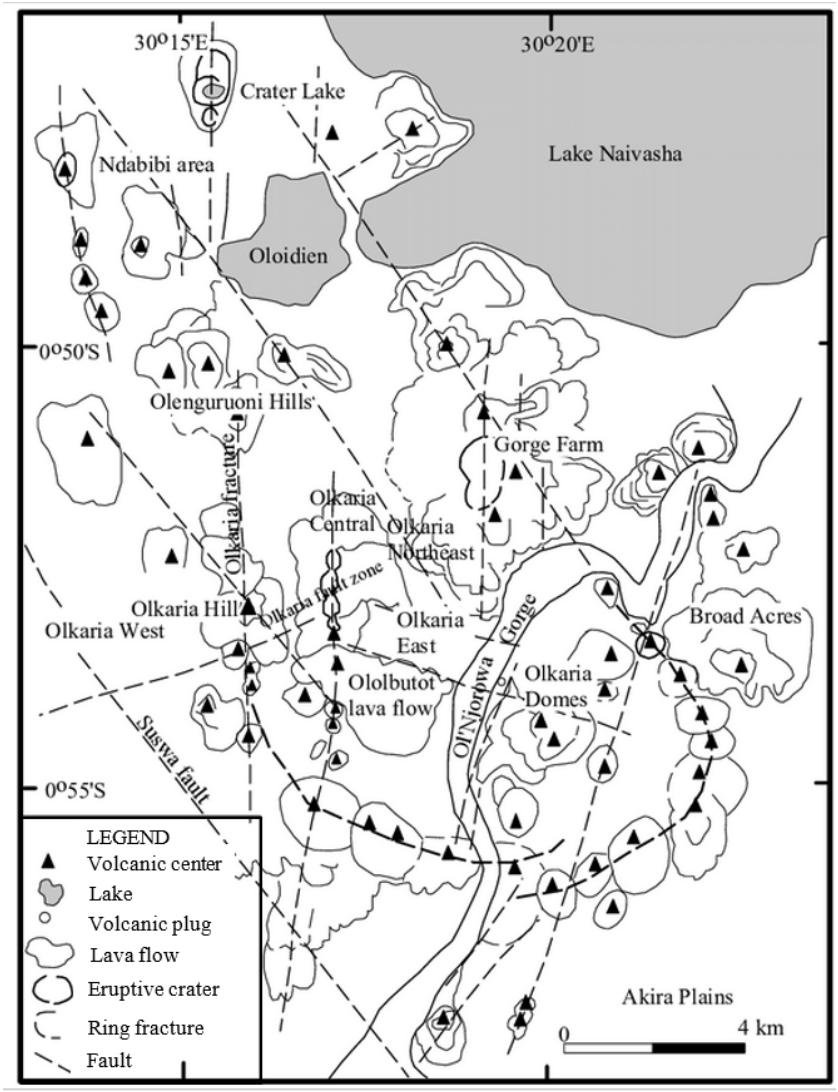

FIGURE 5: Structural map of Great Olkaria Volcanic Complex (Clarke et al., 1990)

The Olkaria fault zone represents the E-W faults. This fault intersects the Suswa Fault in the west and is buried by the young Ololbutot lavas towards the centre of the field. Odongo (1993) proposes that this structure is responsible for the permeability properties of the reservoir rocks and controls fluid movement. The Ololbotut and Olkaria N-S faults are considered the youngest and their formation is associated with the recent tectonic activities. Many scholars regard the Ololbotut fault to be still active and some consider it both a recharge zone and a flow barrier dividing the Olkaria field into the eastern and western part (West-JEC, 2009).

Eruption centres in the southeast together with phreatomagmatic craters in the northwest have been used to extrapolate the trace of a rim and evoke the presence of a buried caldera (Lagat, 2004).

2.3 Geophysical exploration of Great Olkaria volcanic complex

The geophysical analysis of the Olkaria geothermal field has been based on gravity, magnetotellurics (TM), magnetics, micro-seismology and transient-electromagnetics (TEM) data. The gravity survey indicated a dense body between Ol-Njorowa Gorge and the Suswa lineament and dike-like materials have been observed along the N-S Ololbutot fault (Ndombi, 1981). The later has been interpreted as a divide between the eastern and the western part of the Olkaria field and acts as a hydrological barrier between these parts (Lagat, 2004).

Seismic monitoring on the other hand has revealed numerous small, shallow events at the centre of the field whereas deeper events were recorded in the periphery of the field. The events tend to deepen towards the Northeast, Central and Northwest fields, implying that the area is active, but the semi-brittle zone is deeper with no shallow heat source. The shallow and deep events in the Domes and Olkaria northeast fields have been interpreted as volcano-tectonic events and that these two fields may be joined by a NW-SE linear structure (Simiyu and Keller, 1997). This has also been confirmed by the NW-SE trending positive magnetic anomaly along the same structure that corresponds with the main heat source in about 6 km deep with temperatures of above 575°C (Bhogal and Skinner, 1971).

Joint TEM and MT studies have shown three layers of different resistivity. A shallow high resistivity layer at 50-200 m has been interpreted as unaltered formations probably the pyroclastic covers and its thickness varies. The second layer has a resistivity of approximately 15 Ωm, and extends down to 1000 m a.s.l. This layer has been interpreted as the clay cap due to the presence of low-temperature minerals such as zeolites and smectite. Beneath this layer is a high resistivity layer (>100 Ωm) corresponding to the epidote-chlorite zone which has been interpreted as the reservoir of the Olkaria geothermal area. Drilling has confirmed that temperatures within this zone are above 250°C (Wanjohi, 2014).

2.4 Geochemical composition and fluid origin

Geothermal fluid composition studies have been applied in many geothermal fields all over the world for purposes of geochemical exploration and monitoring during production. This is particularly important for establishing the origin and movement of the geothermal fluids as well as to identify the upflow zones. The fluid composition of the Olkaria geothermal field has been reported to vary from one sub-field to another as well as between different parts of the same sub-field. For example, chloride concentration ranges from 50-1200 ppm, H_2S concentration ranges between 3.5-662.6 ppm while bicarbonate concentration ranges from 90-22000 ppm (Kamunya, 2018, Karingith et al., 2010). Karingith et al. (2010) suggests that the abundancy of CO_2 in the system may be controlled by its fluidity to the hydrothermal fluid. High chloride concentrations have been reported in the Olkaria northeast and Olkaria east fields whereas high bicarbonate concentration has been reported in Okaria west, Olkaria domes and the Olkaria Central Fields (Karingith, 2000).

Wells in the Olkaria northeast and Olkaria east fields discharge Na-Cl fluids whereas those in the Olkaria west field discharge bicarbonate rich fluids. The Olkaria central and Olkaria domes fields produce a mixture of bicarbonate and chloride end member fluids (Kamunya, 2014). The origin of the carbonate fluids in the Olkaria northwest and NE of the Olkaria domes field have been interpreted as dissolved carbon dioxide in the recharge waters. The Na-Cl fluids of the Olkaria east and Olkaria northeast fields are structurally controlled and its flow tend to follow the faulting systems, thus the fluid is thought to have a common origin. The Na-Cl fluids of the domes field is however believed to have a source different from the one feeding the Olkaria east and Olkaria northeast fields (Mutua, 2014).

2.5 Temperature structure of GOVC

From fluid chemistry geothermometry, the reservoir temperatures have been estimated and appear to be associated with the tectonic structures. Results from quartz, H_2S and Na/K ratios have indicated temperature ranges of 150-260°C in the Olkaria Central field, 175-260°C in Olkaria West, and 170-285°C in the Olkaria Domes field. The Olkaria East and Olkaria Northeast field on the other hand show temperature ranges of 220-320°C and 200-310°C, respectively (Karingith et al., 2010).

While analysing the temperature and pressure profiles of the wells in the Olkaria geothermal field, Rop (2013) observed the presence of three key heat sources below the Gorge Farm volcanic centre, the Olkaria domes field and Olkaria hill. He went further to state that heat source below the Gorge Farm volcanic centre is responsible for the upflow zones of the Olkaria east and Olkaria northeast fields while

the one below the Olkaria hill is associated with the northwest field upflow zone. These upflow zones appear to be oriented along the NE-SW and NW-SE faults within these fields. The Ololbutot and the ring structure on the other hand act as cold downflow zone (Rop et al., 2018). Temperature reversals have also been observed in the southeast part of the Olkaria domes and in the Olkaria Central fields (Rop, 2013).

2.6 Overview of Olkaria Central field

Surface geology of the Olkaria Central field is dominated by comenditic pyroclastics and alluvial deposits in the northern part. The subfield is bordered by the Olkaria fracture to the west and the Ololbutot fault to the east and is crossed by the Olkaria fault zone in the SE corner. Two unnamed NW-SE trending faults also cut across the Central Field in the SW and NE corners, respectively. The Ololbutot fault has been described as an old rejuvenated fault and is responsible for shallow recharge in the area. The NW-SE faults are the oldest within the rift and provide deep recharge in this sector. Wells in the Olkaria Central Field discharge liquid-dominated fluids that are a mixture of NaCl bicarbonate fluids (Opondo, 2015). Temperatures range from 150-260°C which is the lowest compared to the other sub-fields. There is no nearby heat source in this sector and temperature reversal has been reported in OW- 201 (Omenda, 1998).

Figure 6 shows a 3D model of the Olkaria geothermal complex constructed by Rop et al. (2018) based on geoscientific observations.

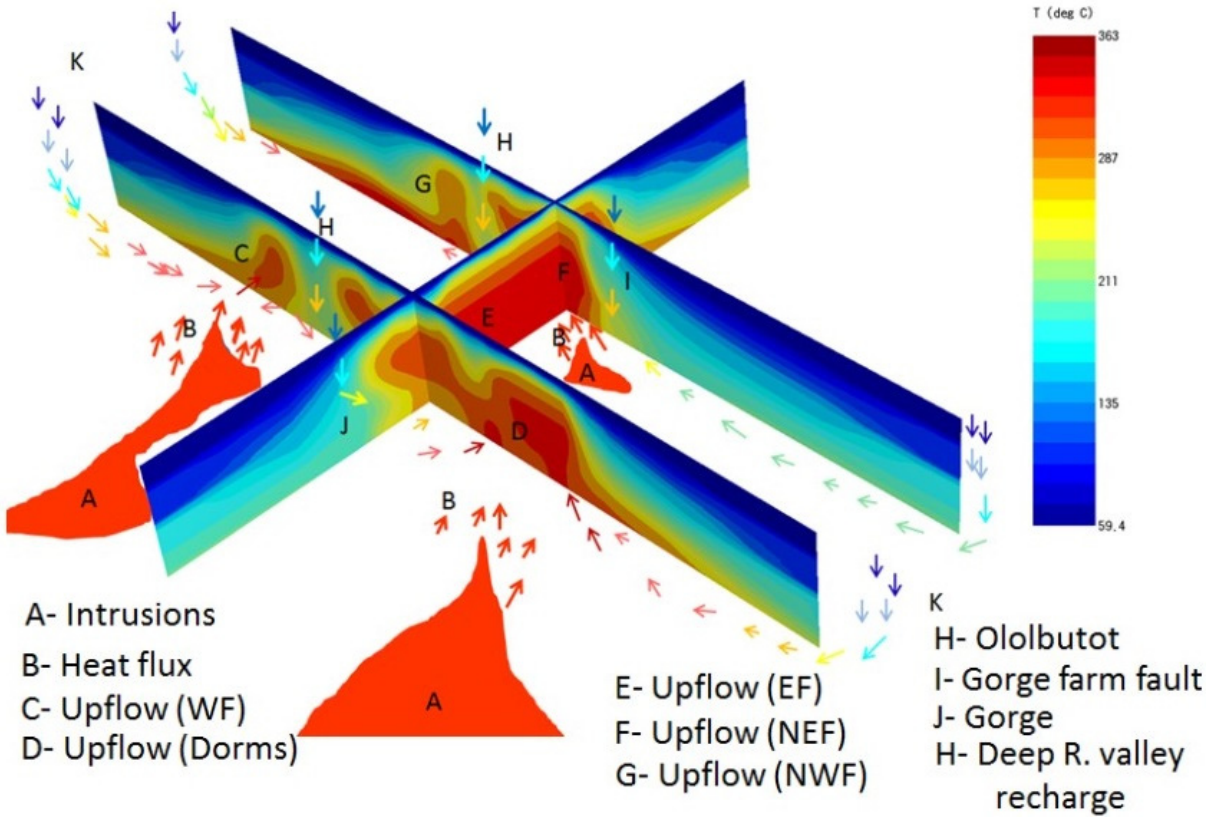

FIGURE 6: 3-D conceptual model of the Olkaria Geothermal Complex (Rop et al., 2018)

3. DRILLING, SAMPLING AND ANALYSIS

3.1 Drilling

Drilling of well OW-205 started on 19th July 2016 and ended on 12th December 2016, lasting a total of 90 days. The well was drilled by KenGen´s rig N370 up to 1158 m depth and later KGN 2 continued to 3000 m. The whole process of drilling spread into four phases as discussed below. A summary of the drilling process is presented in Figure 7.

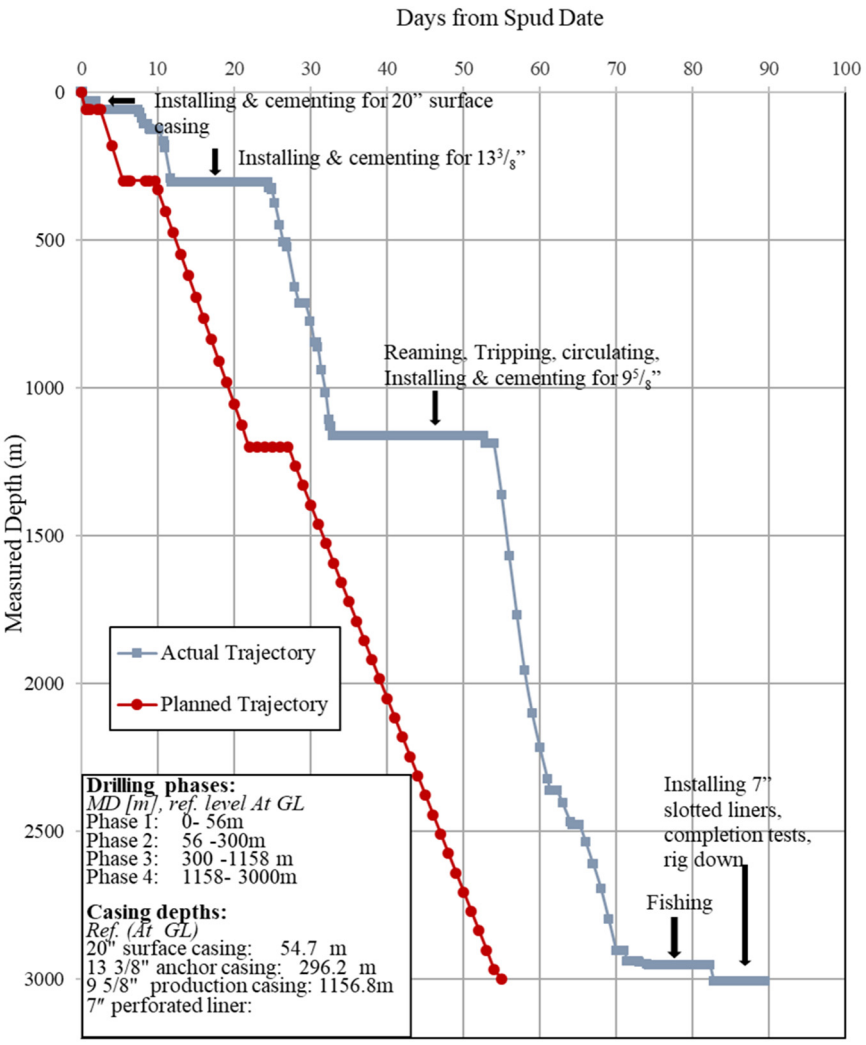

FIGURE 7: Drilling progress for OW-205

Phase 1: Drilling in this phase was conducted using a 26" bit to 56 m depth where the surface casing was installed. Drilling fluids are mud and water. Circulation loses were encountered at 28-56 m. Cementing was done thereafter with two back-fills conducted.

Phase 2: A 17½" bit was used in this phase. A 13⅜" anchor casing was installed at 300 m. Loss of circulation returns was experienced throughout the entire depth range except for 66-68 m. Cementing was conducted subsequently and was confirmed successful after the 11th backfill. Drilling fluids in this phase were water down to 160 m, aerated water, foam and air were introduced from 160 to 300 m depth.

Phase 3: In this stage, drilling was done using a 12¼" bit to 1158 m with aerated water and foam as drilling fluid. While only partial circulation returns were retrieved for most depths' ranges, there was good recovery between 698-1014 m and total loss of returns from 754-826 and 1014-1016 m. A 9⅝" production casing was installed at 1158 m.

Phase 4: This phase involved drilling with an 8½" bit and installation of the 7" slotted liners. The 3000 m well depth was reached on 14th December 2016 ending the drilling process. This phase was characterised by good cutting recovery with a major loss of circulation zone from 2176-2252 m depth.

3.2 Sampling

Due to ease of recovery and low cost compared to coring, drill cuttings have been and are still the standard borehole rock samples and a favourable source of downhole information used in subsurface geological studies. Sampling of rock cuttings for OW-205 was done at 2 m intervals and where the

samples were inadequate or unrepresentative 4 m interval cuttings were sampled. However, in zones where partial or total loss of circulation was experienced, no samples were collected. Samples were then labelled with well name and sample interval. Similar information was recorded in the sampler's notebook for future reference.

3.3 Analytical techniques

Once the rock cuttings have been collected, preliminary analysis takes place at the rig by the rig site geologist, then they are cleaned and stored for further analysis in the laboratory. Below is a brief discussion of some of the common analytical procedures that are used for cutting analysis in this well.

Binocular analysis: This is the initial analysis and is commonly done at the rig site by the rig site geologist for quick understanding of the subsurface geology and the geological conditions**.** It involves studying the samples under a binocular microscope. Before the analysis, the cuttings were put in a petri dish, washed in clean water to remove mud and other drilling fluids as well as to enhance visibility. Useful information and rock properties such as colour, grain size, rock type, alteration type and intensity, veining, fracturing etc., are noted at this stage. This information is helpful for estimating the well temperatures, determining production casing depth and to forestall drilling problems related to collapsing formations and swelling clays.

Petrographic analysis: Petrographic analysis involves viewing the samples in a thin section (glass slide) using a petrographic microscope. Representative samples were selected from various depths throughout the well and thin sections were prepared. Fifty-five thin sections of OW-205 were prepared and analysed to confirm the rock type, alteration mineralogy and intensity, mineral alteration sequence, permeability and any other additional observation not achieved under the binocular microscope. A Leica DM 2700P petrographic microscope was used and mineral properties were described based on the thin section microscopy guidelines given in Raith et al. (2012) and Kerr (1959).

X-ray diffraction analysis: Although other analytical methods have been instrumental in identification of clays, XRD is by far the best method for clay analysis. This analytical technique is used to supplement the above discussed techniques, particularly for identifying fine-grained clays. Fifteen samples from OW- 205 were used for this analysis. Two grams (2 g) of each sample were washed carefully using distilled water, then put in a test tube filled with distilled water. The content was shaken for approximately 4 hrs (to form suspension), then left to set for 10 minutes. Few drops of the suspension were put on a glass slide and left overnight to dry in ambient temperature and humidity. These were the untreated samples and were measured in the XRD machine and marked UNT. After the measurement the samples were placed inside a closed desiccator, filled with ethylene-glycol. The samples were left in the ethylene-glycol fume for 24 hours and then measured (GLY, glycolated). Finally, the samples were heated in a furnace for about 1 hour in 550°C and after cooling measured again (HIT, heated). The set of three measurements were then viewed superimposed using special software for X-ray diffraction data display (Bruker, Diffra.Eva).

Each sample was measured from $2\Theta=2°–14°$ in 0.02° increments (steps) and measured for 1 second in each step. Each set-up was saved in parameter file leir-b.dql. Each measurement takes about 10 minutes. The X-ray beam is confined using 0.5° divergence and receiving slits. The equipment used is a Bruker AXS D8 Focus, producing Cu kα radiation with 1.54 Å wavelength at 40 kV and 40 mA. The detector used is a NaI scintillation counter.

Fluid inclusion micro-thermometry: This analysis involves estimation of the homogenisation temperature (Th) which is thought to relate to the temperature of the system at the time of entrapment of the fluid inclusion. This is done using a special stage that allows heating and cooling over a wide range of temperatures between 200-1500°C. Two phase inclusions are heated until uniformity is achieved. This is the homogenisation temperature and is estimated to be the lowest temperature at which the inclusion formed (Randive et al., 2014).

Prior to the analysis, clear/translucent, euhedral crystals of calcite were picked from the rock cuttings at 1238 m (with the help of the binocular microscope). The grains were then mounted on a glass slide using a Crystalbond^{TM} or superglue. The samples were then polished using 800, 1200 and finally 4000 grit sandpapers. After this they were released from the glass by putting it in an acetone filled beaker and agitating it in ultrasonic cleaner for 10-15 minutes. This process was repeated to the other side of the grains until a final thickness of less than 100 microns was reached. The grains were again released from the slide using ultrasonic clear as explained above and were ready for analysis. The samples were then mounted in a Linkam TMS94 heating stage that is connected to a Leitz Laborlux 12 microscope and the images are viewed on the computer using a streaming software called Olympus Stream Start. The samples were then heated steadily until the homogenisation temperature (Th) was attained.

4. RESULTS

4.1 Lithology

The lithological sequence was constructed using information obtained from both binocular and petrographic studies. Below is a detailed description of the units and a visual presentation can be found in Figure 8. Note that missing depths represent loss of circulation returns.

4.1.1 Upper Olkaria volcanics 0-686 m

These constitute the surface rocks and represent the latest volcanic activities. The formation comprises of pyroclastics, comendites, trachytes and minor basalts.

0-28 m – Pyroclastics: They form the upper most section of the well and are composed of brown to grey, heterogeneous ash-fall deposits comprised of soils, glass, pumice, obsidian and lithic fragments of weathered lava. The matrix is fine to medium grained and vesicular. The exact origin of this pyroclastic fall is not known, yet but some authors suggest that most of it may have originated from Longonot and some from Suswa and Olkaria. Except for mild oxidation caused by the interaction of oxygen-rich groundwater, no hydrothermal alteration minerals were observed in this unit. Total loss of circulation was encountered, and no cuttings recovered from 28-366 m depth.

366-370 m – Rhyolitic tuff: Heterogeneous rhyolitic tuff, white to light brown, fine grained to cryptocrystalline with quartz and minute fragments of rhyolitic lava embedded in the matrix. It is slightly porous with vesicles filled with pyrite, zeolites and quartz.

396-434 m – Rhyolite: Grey to brown, fine-grained, porphyritic rhyolite with mainly euhedral and subhedral quartz and feldspar phenocrysts with minute mafic minerals in the rock matrix. The unit is vesicular, and the brown colour is attributed to the mild oxidation and the infilling of the vesicles by brown clays. Numerous loss zones of 4-10 m are encountered within this depth.

434-436 m – Trachytic tuff: Dark grey, fine-grained trachytic tuff with sanidine phenocrysts. It is porous, mildly oxidized and highly heterogeneous with lithic fragments of cryptocrystalline trachyte. Vesicles are filled with clays.

466-472 m – Trachyte: Fine-grained to cryptocrystalline, porphyritic trachyte which is mildly oxidized and vesicular. The unit is slightly heterogeneous due to tuff fragments. Alteration minerals observed in this unit are clays, amorphous silica and pyrite.

494-566 m – Trachyte: This trachyte unit is like the one above but is moderately porphyritic with mainly euhedral to subhedral sanidine phenocrysts embedded in groundmass of tabular microlites of sanidine

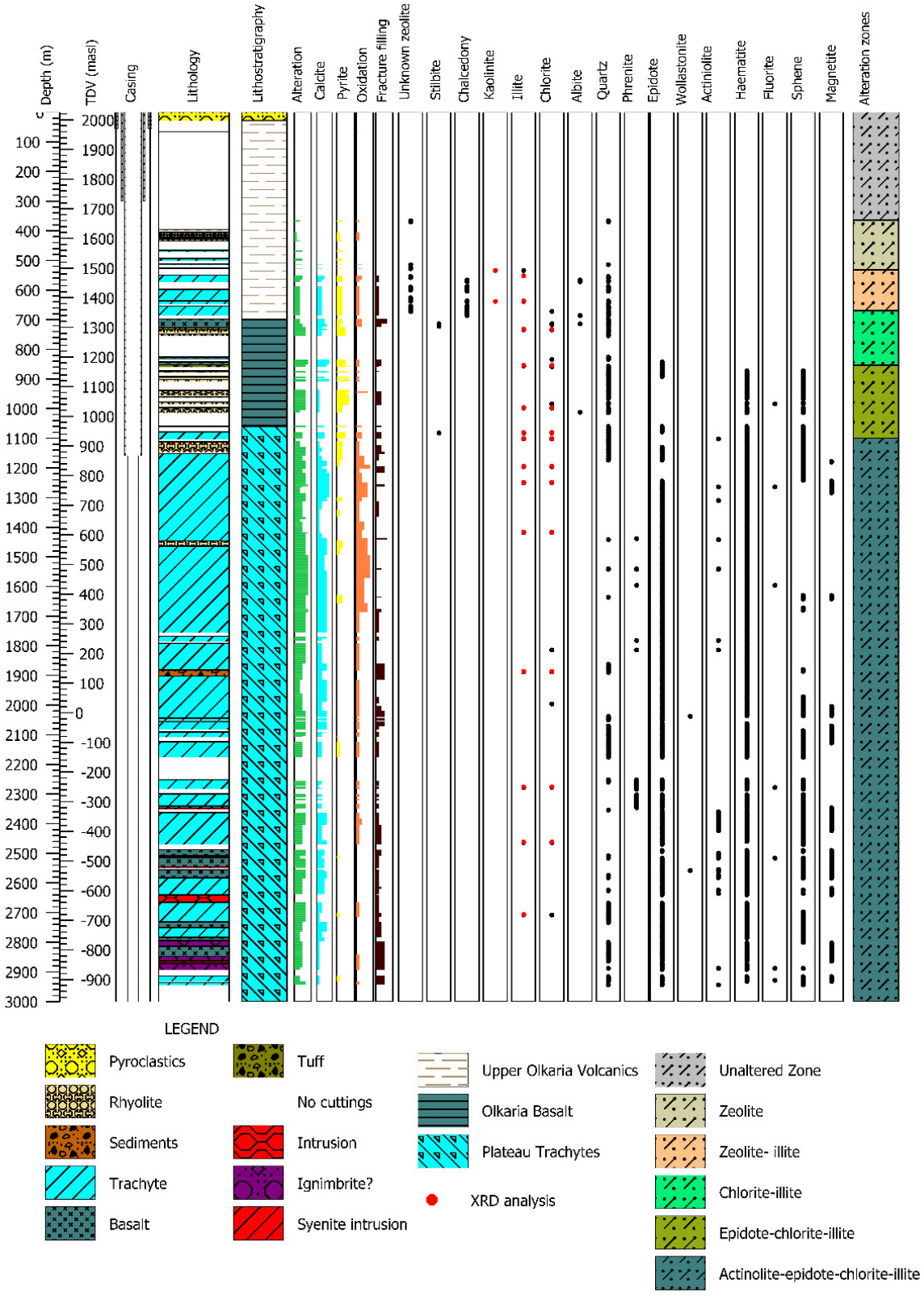

FIGURE 8: Lithology, hydrothermal alteration mineralogy and alteration zonation of well OW-205, Olkaria Central field

and quartz. The unit is slightly vesicular with infills of pale green clays and occasional tiny veinlets filled with quartz. Minor zones of lost circulation returns are encountered within this zone.

566-686 m – Trachyte: Brown-grey to pinkish trachyte which is fine grained and highly porphyritic with sanidine phenocrysts. Phenocrysts are relatively large compared to the trachyte above. Slightly vesicular trachyte with vesicles filled with clays and quartz. Moderate alteration to green clays is observed in fine-grained matrix. Minor zones of circulation loss occurred within the section.

4.1.2 Olkaria basalts 698-1060 m

This formation comprises mainly of thin layers of basalt intercalated with thin layers of tuff, trachyte and rhyolite. The basaltic lavas are commonly fine grained, hypocrystalline and porphyritic with phenocrysts of plagioclase, augite and minor opaque minerals. This formation represents the cap rock of the geothermal reservoir.

698-726 m – Basalt: This unit is dark grey to brownish grey, fine grained, hypocrystalline, dense with few phenocrysts of plagioclase and pyroxene (augite) and scarce olivine phenocrysts with disseminations of opaque minerals in the matrix. The unit is vesicular and slightly veined with calcite and quartz infilling vesicles and veins. Generally, the unit is moderately hydrothermally altered.

726-734 m – Basaltic tuff: This unit is brown, fine grained, heterogeneous and composed of sub-rounded fragments of volcanic glass fragments, clastic sediments and basaltic fragments conspicuously embedded in an aphanitic matrix.

768-772 m – Basalt: Thin layer of basalt which is heterogeneous and mixed with rhyolite tuff and trachyte fragments. Basalt is grey, fine grained with sparse phenocrysts of plagioclase and pyroxene. It is vesicular with infills of quartz, pyrite and clay. Calcite observed in rock matrix.

826-834 m – Basalt: Brown grey, fine-grained, porphyritic basalt with plagioclase and pyroxene phenocrysts. Vesicular basalt with infills of clays, calcite and pyrite. Veins filled with calcite observed. Unit is mixed with trachyte and tuff fragments at 842-852 m. First appearance of crystalline epidote at 842 m. Epidote superimpose calcite in vesicle. Platy calcite observed. Hydrothermal alteration is moderate. Partial loss of circulation observed within the section.

852-878 m – Basaltic tuff: Heterogeneous, brown-grey to pale green, fine-grained basaltic tuff with fragments of clastic sediments and basalt embedded within the matrix. Unit is porous with infills of calcite, quartz and clays. Calcite is abundant in rock matrix. High hydrothermal alteration.

892-908 m – Rhyolitic tuff: Heterogeneous, whitish grey, fine- to medium-grained, xenomorphic rhyolitic tuff with abundant quartz and feldspar in matrix. Fine-grained, euhedral pyrite crystals disseminated in rock matrix. Porous rock with infills of clay minerals. Hematite and sphene are first observed at this depth.

938-982 m – Rhyolite: White-green, fine-grained, porphyritic rhyolite with quartz and feldspar phenocrysts. Opaque minerals in groundmass exhibit flow texture. Abundant pyrite observed at 942-946 m while unit is fractured and highly oxidised at 944-948 m but veins and vesicles are infilled with haematite, clay and quartz. Some open vesicles observed at 978-982 m.

982-1014 m – Heterogeneous tuff: Heterogeneous tuff with fragments of rhyolite and basalt. Tuff is composed of brown-green, fine-grained matrix with feldspar and quartz. Vesicles in rhyolitic and basaltic fragments have infills of green clays.

4.1.3 Plateau trachytes 1060-3000 m

This formation forms the bulk of the reservoir rock in this well. It comprises mainly of trachytes with minor intercalations of rhyolite, tuff, and basalts. Trachytes in the plateau suite occur in two varieties; aphyric type which is fine grained with abundant feldspar microlites and the porphyric type with sanidine phenocrysts. Granitic and syenitic intrusions are observed at depth.

1060-1062 m – Tuff: Red brown, fine-grained and highly oxidised tuff. Vesicular tuff with infills of green clays, epidote, calcite and secondary quartz.

1078-1102 m – Trachyte: Grey, fine-grained trachyte with euhedral sanidine phenocrysts. It is vesicular and veined with infills of calcite, haematite and quartz. The unit is fractured with pyrite disseminations. Sporadic circulation loss observed within interval.

1112-1130 m – Rhyolite: White-pale green, fine-grained, quartz-rich rhyolite with equigranular quartz and feldspar matrix. Rhyolite contains sparse quartz and sanidine phenocrysts. Spherulites are observed at 1126-1128 m. Rhyolite has some vesicles and is veined with infills of green clays, quartz and haematite.

1130-1148 m – Heterogeneous rhyolite: This unit is the same as above but becomes highly heterogeneous with basalt, tuff and trachyte fragments.

1152-1254 m – Trachyte: Light grey-brown, fine-grained, porphyritic trachyte with sanidine phenocrysts. Vesicular trachyte with infills of green clays. Sanidine phenocrysts are altered to green clays. Trachyte exhibits flow texture with disseminations of pyrite in rock matrix. Micro-veins are filled with pyrite, green clays, calcite, and epidote. Very high intensity of alteration at 1248-1254 m. Platy calcite, haematite and sphene are abundant. The formation is highly magnetic.

1254-1300 m – Trachyte: Grey-brown, fine-grained, crystalline, aphyric trachyte with sanidine laths in matrix. Abundant epidote at 1256-1260 m. Abundant sphene, haematite and magnetite observed. The unit is highly oxidised.

1300-1446 m – Trachyte: Brown-grey, fine-grained aphyric trachyte with sporadic subhedral sanidine phenocrysts. Highly oxidised intervals at 1348-1364 m and 1408-1412 m where primary minerals in the matrix cannot be recognised.

1446-1464 m – Rhyolite: Heterogeneous, white-green, fine grained, porphyritic rhyolite with quartz and feldspar phenocrysts. Rhyolite is highly altered to pale green clays.

1464-1882 m – Trachyte: Brown-light grey, fine-grained, aphyric and holocrystalline trachyte. Scarce subhedral sanidine phenocrysts are observed. Abundant epidote at 1558-1562 m. Thick homogeneous unit which is highly oxidised at 1490-1546 m and 1582-1586 m indicating possible zones of mixing with cold fluids. Platy calcite observed at 1672-1708 m. Minor zones of circulation loss are encountered within this zone.

1882-1902 m – Sediments: Greyish green, cryptocrystalline sediment with tiny dark green spots and with no visible banding or flow texture. The unit has relatively high silica content, suggesting lake deposit or ash-fall deposit that have undergone silicification due to invasion by silica rich hydrothermal fluids. This is confirmed by the presence of secondary quartz in tiny veinlets throughout the unit. The formation is highly altered to green clay minerals resulting to the varied shades of green that this section displays.

1902-2340 m – Trachyte: Light grey to brown, fine-grained, porphyritic trachyte with sanidine phenocrysts. Trachyte is moderately to highly altered. Alteration intensity increases with depth and

becomes very high from 2066-2136 m where the rock becomes green due to alteration of feldspars to epidote (epidotisation). Minor losses encountered within this section.

2340-2348m – Basalt: Dark grey-green, fine-grained, porphyritic basalt with elongated phenocrysts of plagioclase feldspars. The unit appears dense and holocrystalline with specks of opaque minerals. Calcite filled veins, magnetite and sphene are common in this unit.

2348-2352 m – Granitic intrusion? White, fine- to medium-grained granitic dike which is slightly vesicular, moderately porphyritic with quartz phenocrysts. It is relatively fresh with hematite filling some vesicles while fine-grained sphene aggregates are sparsely disseminated in the matrix.

2362-2470 m – Trachyte: Grey, fine-grained, porphyritic trachyte with distinct sanidine phenocrysts. Trachyte is moderately altered to clays with micro-veins filled with sphene minerals. Platy calcite is abundant.

2488-2546 m – Basalt intrusion: Dark grey, fine-grained and porphyritic basalt with elongated phenocrysts of plagioclase feldspar. The basalt appears dense and holocrystalline with specks of opaque minerals. Calcite filled veins while magnetite and sphene are common in this unit. A thin layer of light brown, fine-grained to glassy trachyte is noted between 2508-2514 m.

2546-2550 m – Granitic intrusion: Similar as intrusion above at 2348-2352 m but with microscopic, brown, elongated needle-like mafic minerals. No hydrothermal alteration minerals observed.

2556-2582 m – Basaltic intrusion: Dark grey, fine-grained, porphyritic basalt with euhedral elongated phenocrysts of plagioclase feldspar. The basalt appears dense and holocrystalline with specks of opaque minerals. Calcite filled veins while magnetite and sphene are common in this unit. Calcite disseminations in rock matrix.

2582-2640 m – Trachyte: Light grey, fine-grained, porphyritic trachyte with distinct subhedral sanidine phenocrysts. Feldspar rich trachyte with holocrystalline groundmass. Feldspar is altered to brown and pale green clays. Abundant veins filled with clays observed at 2616-2640 m. Platy calcite observed.

2640-2666 m – Granitic intrusion: Similar to granitic intrusion at 2546-2550 m. Light grey, medium-grained and relatively fresh granite with quartz, feldspar and minor mafic minerals. It is a relatively massive unit and moderately porphyritic with distinct quartz and feldspar phenocrysts. Elongated needle-like mafic crystals are smaller in size than in granitic dike at 2546-2550 m.

2666-2732 m – Trachyte: Grey, fine-grained, vesicular trachyte with occasional sanidine phenocrysts. Alteration of felsic mineral to epidote is evident. Micro-fracturing is observed with fractures filled with felsic and mafic minerals. Vesicles are infilled with quartz.

2732 -2750 m – Basaltic intrusion: Similar as basaltic dike described at 2556-2582 m with abundant veins infilled with calcite and green clays. Abundant veins observed.

2750-2814 m – Trachyte: Similar trachyte as at 2666-2732 m. Veins with infills of clays and epidote. Veining is relatively abundant compared to other depths.

2814-2848 m – Basaltic intrusion: Similar as basaltic intrusion described at 2556-2582 m with veins filled with quartz and calcite. Veining is relatively abundant.

2848-2864 m – Ignimbrite?: The formation is green, very fine-grained, silica rich with minute crystals of quartz. It is characterised by white irregular patches, comprised of feldspar and quartz which have almost the same texture as the rock matrix. Smaller patches, however, look like anhedral feldspar phenocrysts, thus exhibiting a xenomorphic texture. It is however difficult to tell if these patches are

fiamme or not due to their irregular morphology. In thin sections the rock exhibits spherulitic texture where elongated crystals of quartz and feldspars appear to radiate from a nucleus. Another suggestion for the cause of these patches would be patchy alteration or recrystallization due to changes in pressure, temperature or the fluid environment. Minute veinlets infilled with quartz are common in this formation.

2864-2872 m – Syenitic intrusion: Whitish, medium- to coarse-grained, granular syenite with distinct euhedral sanidine phenocrysts. It is dense and appears relatively fresh with minor amounts of clay minerals.

2872-2894 m – Ignimbrite?: Similar unit as described at 2848-2864 m.

2914-2944 m – Trachyte: Grey, fine-grained, porphyritic trachyte with moderate amounts of sanidine phenocrysts. Fractured unit with fractures infilled with quartz, epidote, and green clays. Euhedral pyrite and platy calcite observed. Total loss of circulation to 3000 m.

4.2 Hydrothermal alteration

Hydrothermal alteration is a term used to describe the many processes through which primary rock forming minerals change their physical and chemical properties due to reactions associated with the flow of hot fluids along fractures and grain boundaries (Reed, 1997). Primary minerals usually form in sequential groups determined by the physical and chemical conditions under which the magma solidifies. Alteration of these pre-existing minerals through hydrothermal processes results in secondary minerals. Some of the hydrothermal processes involved are ion exchange, dilution, replacement, recrystallization and precipitation. These processes take place in environments where key factors such as temperature, pressure, water-rock ratio, chemical nature of the fluid and that of the wall-rock as well as the physical nature of the wall-rock are at play (Schwartz, 1950, Browne, 1984). Temperature is considered the most significant factor since most reactions are attained at elevated temperatures and most minerals are thermodynamically stable at specific high temperatures (Lagat, 2004). The duration of the interaction between the fluid and the rock is equally important.

Cutting analysis for this well was mainly done to identify hydrothermal alteration minerals and relate them to their significance in the geothermal system. A wide range of hydrothermal alteration minerals was identified and a brief discussion on their significance geothermal system is given below. Summary of the same is shown in Figure 8.

Zeolites are a temperature dependent calc-silicate mineral that occur at temperatures between 40-120°C. Unidentified zeolites were common between 366-650 m, occurring as white radiating crystals in clusters. In the thin section, stilbite was observed in vesicle at 712 m as colourless spherulites with very low birefringence and perfect cleavage on (010).

Chalcedony was observed filling vesicles in trachyte and basalt at 564-686 m. It is a transparent, white to grey amorphous silica with dull lustre. Occurrence of chalcedony indicate stable temperatures of 150-180°C (Kristmanndóttir, 1979), but becomes unstable and recrystallizes to quartz with increasing temperatures.

Kaolinite was identified by XRD analysis at 552 m and 636 m and it is characterised by a peak at 7.1Å in the untreated, glycolated and heated samples. Kaolinite forms in geothermal manifestations at the surface and is also common in soils in hot and moist environments, thus the presence of kaolinite at this depth could reflect a buried surface-soil.

Illite was observed under XRD analysis by peaks between 10.0Å-10.3Å in the untreated, glycolated and heated samples. It was first noted at 552 m and persist to the bottom of the well. The presence of illite usually indicates temperatures of above 200°C.

Chlorite was identified by its characteristic pale green to dark green, fibrous radiating microscopic crystals or anhedral aggregates. Under the petrographic microscope, chlorite was observed at 670 m as pale green crystals with low birefringence, pleochroic with perfect basal cleavage. In XRD analysis, unstable chlorite showed a peak (001) at 14.5 -14.7Å at all three treatments and a peak (002) at 7.1 - 7.2Å for untreated and glycolated samples and a partial or complete collapse of the peak in the heated sample. This is the common type of chlorite in the well and it was first observed on XRD at 732 m and persists down to 2500 m. Stable chlorite had a peak (001) between 14.5-14.7Å and a peak (002) at 7.1-7.2Å after all treatments and occurs only at 1248-1250 m. The presence of this clay illustrates minimum temperatures of 220°C. Abundant chlorite was observed between 1152-1284 m and is associated with quartz, epidote, actinolite, prehnite and wollastonite.

XRD results and interpretation for kaolinite, illite and chlorite are presented in Table 1 and Figures 1 and 2 in Appendix I.

Albite forms through hydrothermal alteration of plagioclase and K-feldspars, a process commonly known as albitization. It was identified in petrographic analysis as whitish to grey (cloudy), translucent with an anhedral to subhedral crystal shape. It displays uneven cleavage with low relief and multiple twinning. Albite was first observed replacing sanidine at 564 m. Its occurrence indicates temperatures of above 180°C at this depth.

Quartz was identified as a transparent, prismatic crystal with hexagonal pyramid shape. In thin sections, it lacks visible cleavage and may show white first order interference colours. The presence of secondary quartz usually indicates temperatures of above 180°C. In OW-205, quartz was observed filling vesicles and veins. It was first observed filling vesicles at 366 m and persisted to the bottom of the well, mainly filling veins and vesicles. Quartz was abundant at 1440 m and 2734-2944 m where it is infilling veinlets, in association with other minerals such clays and epidote.

*Prehnite**:*** This hydrothermal mineral is identified as colourless to grey, translucent clusters of spherical crystals under binocular microscope. It is a nodular and sometimes radial, colourless mineral with second order blue-pink interference colours and may form bow tie structure. Prehnite is formed from geothermal alteration of iron rich minerals and its presence marks temperatures above 240°C. In OW-205, prehnite was observed at 1436 m and 2250-2346 m in associated with chlorite and epidote.

Epidote is an alteration product of feldspar and pyroxene and usually forms at temperatures above 240°C. Under the binocular microscope, epidote is identified as yellowish-green, transparent to translucent crystals with vitreous lustre. In thin sections, epidote is pleochroic with pale yellow in plane light and shows high interference colours on crossed polar. In well OW-205, crystalline epidote was first observed at 842 m. Vein fillings with epidote were abundant at 1248-1296 m, 1418-1440 m and 2505-2580 m while it is less prominent at 1300-1340 m.

Wollastonite: Under the binocular microscope, wollastonite is identified as grey to white, fine fibrous or radiating aggregates with acicular habit. In petrography, it is colourless with first order grey interference colours. The first appearance of wollastonite in geothermal systems marks temperatures of above 270°C. In this well, wollastonite is very rare and was first observed at 2036 m under the binocular microscope and confirmed by petrographic analysis at 2556 m.

Actinolite is an amphibole silicate which appears with varying shades of green and occurs as aggregates of fibrous crystals with radiating structure and vitreous to silky lustre. The green colour is dependent on the amount of iron present in the chemical structure. In thin sections, actinolite exhibit colourless, pale green or deep green pleochroism with moderate relief and good prismatic cleavage. It occurs in association with epidote and wollastonite and may replace pyroxenes or form in veins and vesicles. In this well, actinolite was first observed replacing feldspars at 1100 m and in relatively high quantities at 1440 m and 2514 m depth where it occurs in veins and vesicles. Its presence marks hydrothermal temperatures of above 280°C.

Fluorite was not observed under the binocular microscope but rather with the petrographic microscope. It is an isotropic mineral with perfect cleavage on (111) at 90° and moderate relief. It was first observed at 982 m and persists throughout the well, mainly in vesicles overprinting quartz and calcite, and epidote at 2514 and 2926 m, respectively. It occurs in association with epidote, calcite and actinolite. In Olkaria, fluorite has been suggested to form when cool fluorine rich fluids are heated up to temperatures of about 100-150°C (Leach and Muchemi, 1987). Fluorite forms at temperatures of about 130-150°C. In other peralkaline regions, fluorite deposition has been associated with dilution of brine with cool, Ca-rich meteoric waters, simple cooling of the fluids or mixing of two fluids with different chemical compositions. A temperature decrease on the flow path is the most agreeable explanation (Richardson and Holland, 1979).

Magnetite is an opaque mineral and is easily distinguished from the other oxides by its strong magnetism. It is greyish black colour with metallic and submetallic lustre occurs in aggregates of isometric crystals. In petrography, it is isotropic and displays a brown tint under reflected light. It was observed at 1176 m and persists to the bottom of the well at different depths and is abundant between 2490-2580 m.

Hematite occurs as steel-grey, fine-grained crystals with submetallic to earthy lustre. Optically, it is brownish-red and opaque. It was observed as fine disseminations, vein or vesicle filling throughout the well though with varied intensities. It is abundant between 1418-1838 m, occurring as disseminations in the rock matrix as well as vein filling. The trachytes and rhyolite within this zone are highly oxidised. Like other oxides, the formation of haematite has been associated with conditions where oxygen is readily available.

Sphene forms as a replacement of mafic silicates and was identified as white minute spherical aggregates under the binocular microscope**.** In petrographic analysis, sphene appears dirty brown with very high relief and may form dendritic clusters. This mineral was first observed at 870 m and persist in most parts of the well to the bottom. It was found in abundance from 2086 to 2944 m. At this depth, sphene is seen occurring in vesicles, veins and overprinting high-temperature minerals such as epidote and actinolite. Sphene has been associated with interaction of low temperature (150-200°C) silica undersaturated brine with wall-rock (Salvi and Williams-Jones, 2006).

Calcite and pyrite occur in a wide range of temperatures from 50 to 300°C and 50 >300°C, respectively, thus they cannot be relied on as geothermometers. Their occurrence in a geothermal well, however, is very important since they indicate good permeability. Their description and distribution is discussed as follows.

Calcite is the dominant mineral in this well and was easily identified by its reaction to dilute hydrochloric acid. In the binocular, it appears white to colourless, mostly infilling voids veins and vesicles. Under the petrographic microscope, it is transparent to translucent with pale high order interference colour, perfect rhombohedral cleavage on (1011) at 120°/60° and change of relief with stage rotation. In the Olkaria geothermal field, calcite occurs both as a replacement of rock forming minerals and volcanic glass or as platy. It forms as a result of either boiling, dilution or condensation of carbon dioxide or during the heating of cooler peripheral fluids (Simmons and Christenson, 1994).

Normally, when calcite fills vesicles and fractures, it reduces permeability, but it can reflect previous high permeability. Calcite was observed from 500 m and it persisted throughout the well. Abundant calcite was observed at 832-938, 1216-1300 and 1446-1494 m in basalt and trachyte, respectively, though it was present at other depths in relatively small abundance. Calcite usually disappears at temperatures above 300°C (Nicholson, 1993), thus, its presence to the bottom of the well can imply that the temperatures are below 300°C.

Pyrite occurs as shinny brassy yellow cubic crystals deposited in either fractures, veins or vesicles or as disseminations in the groundmass. In petrographic analysis, it is identified as euhedral cubic crystals

with a brassy yellow lustre under the reflective light. Pyrite is mostly used as an indicator of good permeability in a geothermal system (Lagat 1998). Larger euhedral pyrite crystals and fine-grained disseminations of pyrite in the rock matrix were observed in 744-754, 902-936 and 1152-1158 m. The zone between 744-1152 m has the highest quantities of pyrite compared to all other depths of the well, thus implying that this zone is relatively permeable.

4.3 Hydrothermal alteration zonation

Alteration minerals may form an assemblage which is a chemically stable group and may affect a volume of rock commonly known as an alteration zone (Guilbert and Park, 1986). These assemblages characterize the various hydrothermal-chemical reactions that occur in most active geothermal systems (Hara and Tsuchiya, 2004). During sample analysis, some of the key information gathered include identification of formation temperatures using definite index minerals that form at specific temperatures and maintain their stability within a given range of temperatures. The stability of these minerals and their relationship may be used for indirect estimation of temperature ranges at depth, past or present. This is particularly important when determining the proper depth for installing the production casing. Thus, feed zones that are too cold for production may be cased-out based on the presence or absence of certain index minerals observed during drilling.

In most geothermal fields, minerals used to determine alteration zones include zeolites, mixed layer clays, chlorite, epidote, actinolite and amphiboles (Browne, 1984). In well OW-205, hydrothermal alteration assemblages were successful studied, and five zones were identified (Figure 8). Zonation was defined based on the first appearance of dominant temperature dependent mineral with increasing temperatures and depth.

Unaltered zone (0-364 m): This zone is relatively unaltered with some moderate oxidation noted likely to be associated with the interaction of the formation with percolating waters. The formation mainly consists of pyroclastic deposits and the temperatures are below 50°C and hence do not favour hydrothermal alteration.

Zeolite zone (364-532 m): Identified by the presence of zeolites such as stilbite and other unidentified zeolites that were observed under the binocular microscope and with petrographic analysis. The zone signifies temperatures between 50-200°C. Quartz is also found at 366 m.

Illite –zeolite zone (532-670 m): The presence of illite marks the beginning of this zone. The appearance of illite signifies temperatures of >200°C. Albite and secondary quartz are also found in this zone.

Chlorite-illite zone (670-854 m): This zone is marked by the first appearance of chlorite at 670 m in petrographic analysis and at 723 m in the XRD analysis. Omenda (1998) mentions that the deposition of chlorite occurs at the periphery between cool ground water and rising hot fluids. The occurrence of chlorite indicates temperatures of above 230°C and may indicate the proximity of the reservoir.

Epidote-chlorite-illite zone (854-1100 m): This alteration zone is characterised by the first appearance of epidote at 854 m, observed under binocular microscope. This zone signifies temperatures of >240°C, which is the minimum reservoir temperature for production in Olkaria.

Actinolite-epidote-chlorite-illite zone (1100-3000 m): The actinolite-epidote zone was identified by the first appearance of actinolite at 1100 m, observed under petrographic analysis, and extends to the bottom of the well. Actinolite is a temperature dependent hydrothermal mineral indicating temperatures of >280°C. Other minerals found in this zone include chlorite and epidote.

4.4 Hydrothermal mineral paragenesis

Mineral paragenesis can be described as the sequence in which hydrothermal minerals are deposited. As mentioned earlier, hydrothermal temperature-dependent minerals (geothermometers) are key in estimating the temperatures of the geothermal system. When identifying and analysing these minerals, the major intentions are to determine the order of formation in relation to other associated minerals as well as to estimate the conditions under which these minerals were formed. Changes in temperature, pressure and the composition of the hydrothermal fluids may result in precipitation of diverse minerals at different times. This is thus important to interpret the geological history and the different episodes of mineralisation prevailing in a geothermal system, past and present.

Hydrothermal minerals are commonly deposited in veins, vesicles or as replacement products where they occupy the space initially occupied by the former mineral. Several principles have been put forward when determining which mineral is older than the other. For instance, the crystal morphology principle suggests that when minerals with euhedral and subhedral crystals have formed together, the mineral with euhedral crystals is older since its euhedral morphology is associated with growth in an open space when there was no obstruction. The principle of superposition states that minerals that form on top of another are younger that the underlying minerals. Thus, in veins and vesicles, minerals that are lined on the walls are older than the inner minerals. The cross-cutting principle on the other hand states that a veinlet filled mineral is younger than the mineral it cuts across while the mineral that is being replaced is older. With this guidance, it is easier to determine the different temperature regimes in a given geothermal field.

In a stable geothermal system, mineral deposition is prograde where low-temperature minerals deposit earlier then high-temperature minerals. Note that the opposite may suggest a temperature reversal in the system. For this well, the mineral sequence was established at different depths and the results are listed in Table 1 below. Generally, there is good consistence in the deposition from low-temperature alteration minerals to high-temperature minerals, e.g. at 872 m depth where epidote was deposited on chlorite and at 1538 m where actinolite is deposited on quartz. This shows that there is a consistent temperature increase with depth within this zone. A retrograde sequence is observed from 872 m to the bottom of the well. Calcite was deposited on epidote and actinolite at 872 m, 1812 m and 2514 m. Sphene and fluorite were also deposited after high-temperature minerals such as epidote and actinolite at several depths from 2384 m and to the bottom of the well. For instance, at 2886 m sphene was deposited after actinolite. Generally, sphene deposits within a wide range of temperatures (200 - >300°C), therefore, its deposition after actinolite only confirms that the temperatures are above 200°C.

TABLE 1: Hydrothermal mineral paragenesis

Depth (m)	Order of deposition	Occurrence
832	Quartz >> Calcite	Vesicle
872	Chlorite>>Epidote>>Calcite	Vesicle
1262	Quartz>>Calcite	Vesicle
1538	Quartz>>Actinolite	Vesicle
1812	Epidote>>Calcite	Vesicle
2384	Epidote->>Sphene>>Fluorite	Vesicle
2514	Actinolite->>Chlorite	Vesicle
2514	Epidote>>Sphene>>Calcite>>Quartz>>Fluorite	Vesicle
2622	Actinolite>>Calcite	Vesicle
2886	Calcite>>Actinolite>>Sphene	Vein
2926	Epidote>>Quartz>>Fluorite	Vesicle
2926	Epidote>>Sphene>>Fluorite	Vesicle

Fluorite on the other hand was deposited after epidote from 2384 to 2926 m depth. Fluorite has been associated with the downward movement of cooler fluids (Leach and Muchemi, 1987) and a temperature decrease in the flow path (Richardson and Holland, 1979). Thus, its deposition at these depths may suggest a decrease in temperatures due to the presence of cooler fluids. This signifies the prevalence of two temperature regimes; higher paleo-temperatures and relatively lower present temperatures. Figure 9 shows the deposition sequence from epidote>>sphene>>fluorite at 2926 m.

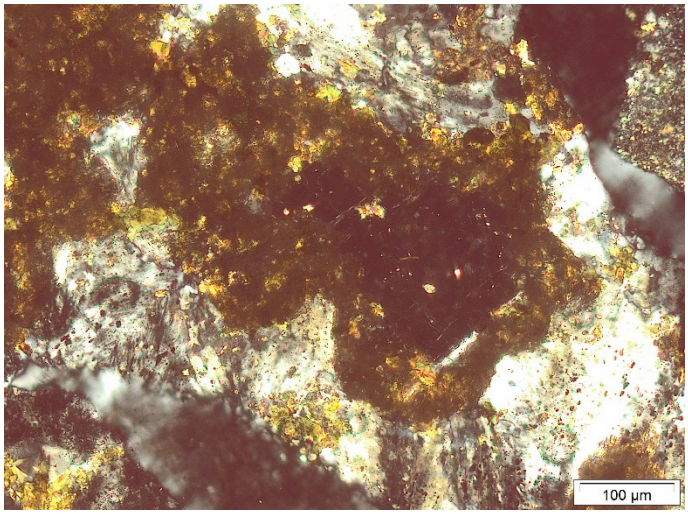

FIGURE 9: Mineral sequence at 2926 m (epidote>> sphene>>fluorite) deposited in vesicle

4.5 Feed zones

A successful production well must intercept hot feed zones. These are underground layers of rock formations that are saturated with water and allow easy movement of water within them. These zones are therefore both permeable, porous and fractured and serve as interaction zones between the well and the reservoir. In volcanic settings feed zones can be found along fractures, faults, intrusions and lithological contacts, as is the case in the Olkaria geothermal field.

Feed zones can be determined using a combination of different methods such as temperature logs, variations in the rate of penetration during drilling, changes of circulation fluid returns (loss/gain), and geological observations. Temperature logs are the primarily method to locate feed zones since it is quick and reliable. It involves injection of cold water into the well, closing the well and allowing it to heat up while measuring the temperature, both during injection and recovery. Geological observations are made during cutting analysis and include determination of lithological contacts, open fractures, veins and vesicles, presence of permeability indicator minerals such as pyrite and calcite, observation of alteration patterns etc. The presence of well-formed (euhedral) crystals of secondary minerals may also indicate good permeability. Other drilling parameters such as weight on bit (WOB) and revolution rate (RPM) for this well were missing, therefore only rate of penetration (ROP) data was used. Under constant drilling conditions, high ROP values may imply that the formation is not compact, thus easily penetrated.

Based on these observations, nine permeable feed zones were identified and categorised as major or minor feed zones depending on their width. A summary of the findings is presented in Table 2 and Figure 10. The upper feed zones (1-3) were cased-off because the temperatures at these depths were not high enough and would therefore interfere with the productivity of the well.

Feed zone 4 at 1182-1402 m is a major feed zone characterised by high intensities of high-temperature minerals such as epidote and actinolite with pyrite and calcite in abundance. There is moderate veining of the formation though some veins are filled with secondary minerals such quartz, calcite, pyrite and haematite. This feed zone, however, causes a regression on the temperature logs. The high intensities of unstable haematite deposited in veins, vesicles and as disseminations in the rock matrix may indicate a possible feed of cooler fluids. Zones of high oxidation/bleaching are also found at 1190-1200 m and 1248-1300 m, indicating the interaction with oxygenated fluids in this section.

Feed zone 5 between 1784-2124 m is a major zone characterised by high intensities of high-temperature minerals such as epidote and actinolite as well as high intensity of veining and fracturing. Veins and vesicles in this section are filled with epidote, calcite, quartz and actinolite. There is a noticeable temperature decrease within this zone, thus indicating another possible zone with cooler fluids.

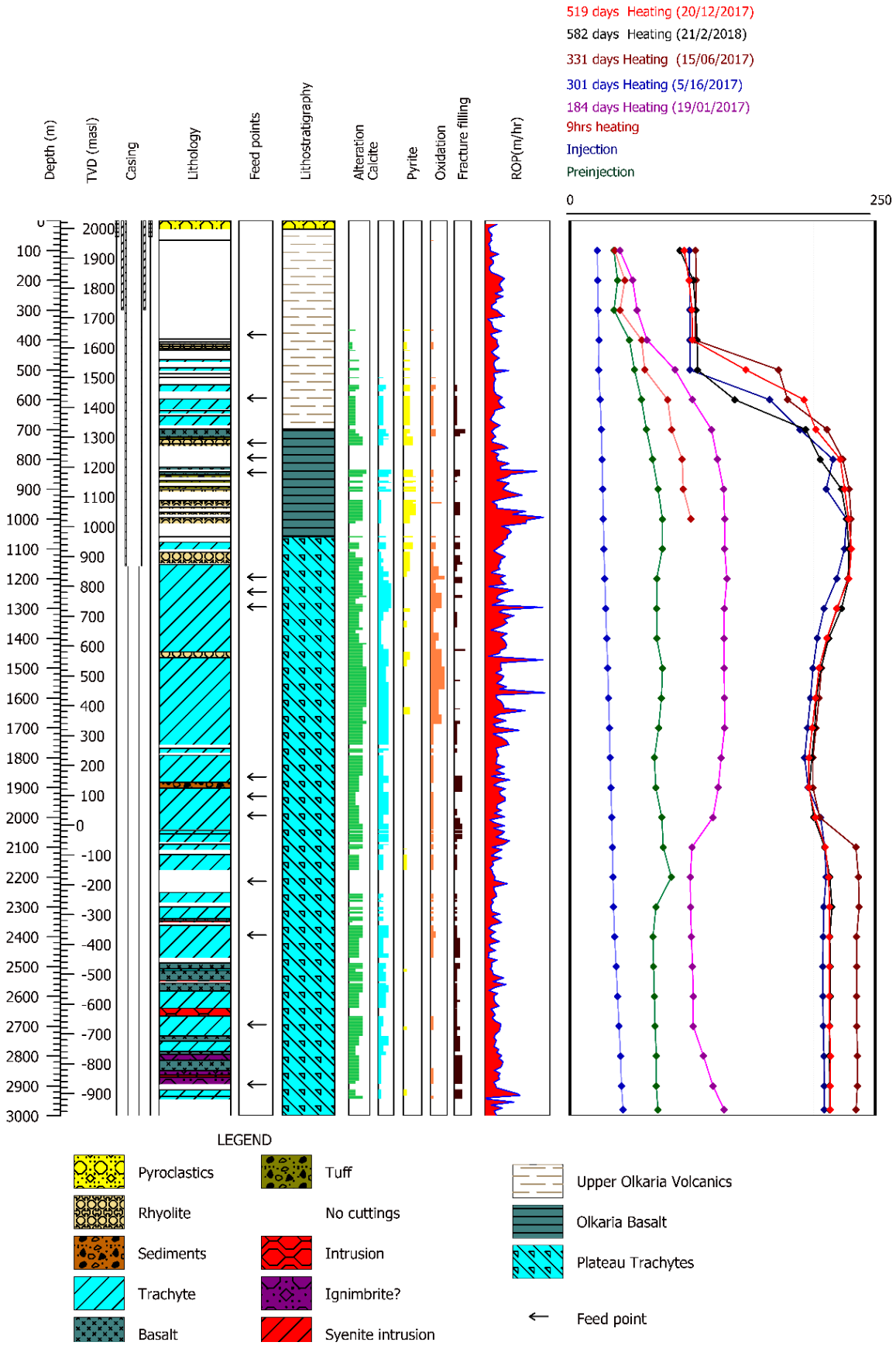

FIGURE 10: Lithology, temperature profiles and feed zones of OW-205

TABLE 2: Interpreted feed zones based on different observations

	Depth (m)	Aquifer category	Rock type	Evidence from observations
1	370-406	Minor, cased off	Rhyolite / tuff	Vesicles, increased oxidation, loss of returns at contact between rhyolite and tuff
2	726-748	Minor, cased off	Basaltic tuff	Lithological contact, fracturing, vesicles, lost circulation, increased oxidation, abundant pyrite
3	754-978	Major, cased off	Rhyolite/basalt/tuff	Multiple lost circulation returns at litho-contact, abundant pyrite and calcite, veining, vesicles, increased alteration
4	1182-1402	Major	Trachyte/rhyolite	Lithological contacts, high alteration intensities, veining, high oxidation, vesicles, lost circulation returns, abundant calcite and pyrite
5	1784-2124	Major	Trachyte	High alteration intensities, veining, abundant calcite, multiple loss zones, fracturing
6	2174-2224	Minor	Trachyte	High alteration, veining
7	2470-2508	Minor	Trachyte/basalt	Intrusion related, high alteration intensities, veining
8	2666-2732	Minor	Trachyte/granitic intrusion	Intrusion related, high alteration intensities, veining, fracturing
9	2894-2944	Minor	Trachyte/granitic intrusion	Fracturing, veining, pyrite, intrusion related

Feed zones 6-9 are minor zones and are characterised by both high-temperature alteration minerals, intensive veining and fracture filling while feed zones 7 and 8 have intrusion related permeability. Sphene and calcite are common in this section, filling vesicles and veins alongside epidote and actinolite. The section has a positive influence on the temperature logs, thus indicating the presence of hotter fluids and increased formation temperature around this section. Cooler fluids are heated by convection as they move into deeper aquifers. The fluids are heated until they reach a stable temperature of around 210°C from 2200 to 3000 m depth. This is the zone where the reservoir temperatures and those of the well are at equilibrium.

4.6 Fluid inclusion micro-thermometry

Fluid inclusions are small volumes of liquid and/or gases that are trapped within crystals of minerals. These paleo-fluids offer crucial information about the geological conditions and processes that prevailed during the time of entrapment. The study of these inclusions therefore reveals important geological information such as temperature, salinity, pressure etc., thereby giving insight into the paleo-conditions under which the rocks and minerals formed (Randive et al., 2014).

Fluid inclusion micro-thermometry for this well was based on one calcite crystal picked at 1238 m. The crystal was heated while monitoring the behaviour of the entrapped fluids and the homogenisation temperature (T_h) was recorded as the minimum temperature of entrapment (Figure 11). Forty-

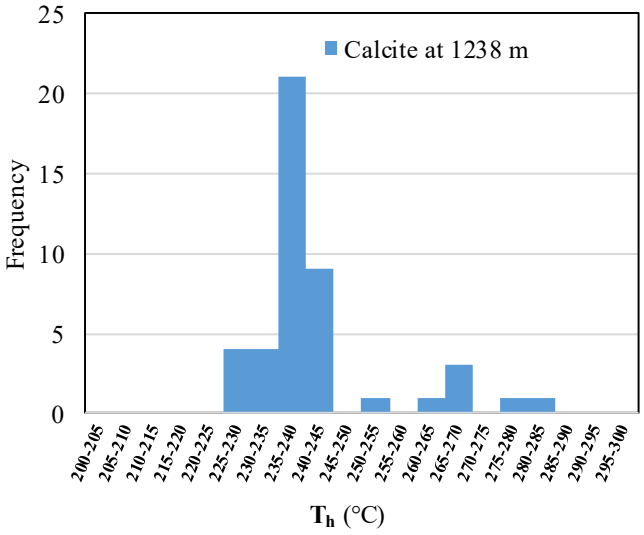

FIGURE 11: Graphical presentation of the homogenisation temperature distribution

five inclusions were analysed, and the results revealed a temperature range of between 225 and 285°C with a stabilisation temperature of 235-245°C.

It was not distinguished if these temperatures are from primary, secondary or pseudo-secondary inclusions but it can be speculated that there existed two distinct thermal regimes around this well. The first regime is that of high temperatures of around/above 285°C which may also be interpreted as the paleo-temperature. The second regime is the low-temperature regime of around 225°C and may be interpreted as the present temperature. The present temperature coincides very well with the measured temperature which is 225°C at 1240 m.

4.7 Thermal history

Study of the thermal history is key in understanding the reservoir conditions, past and present. This is achieved by analysing the patterns of the past and present temperature. In this well, temperature analysis and comparison were made by comparing the alteration mineral temperature curve, measured temperature after 582 days recovery, the boiling point curve and the homogenisation temperature from fluid inclusion analysis of calcite as shown in Figure 12. The alteration mineral temperature curve was plotted using temperature dependent minerals and the depth at their first appearance. This temperature indicates the minimum paleo-temperatures at which these minerals were formed. Index minerals include quartz (>180°C), illite (>200°C), chlorite (>230°C), epidote (>240°C) and actinolite (>280°C). The heating up profile for 582 days recovery show the present temperature since it was taken after a long period of time when the well had fully recovered from injection during drilling. The homogenisation temperature based on fluid inclusion analysis of calcite ranged between 225-285°C with a stabilisation temperature of 235-245°C. Downhole pressure and boiling point curve relative to the current water level in the well was also plotted.

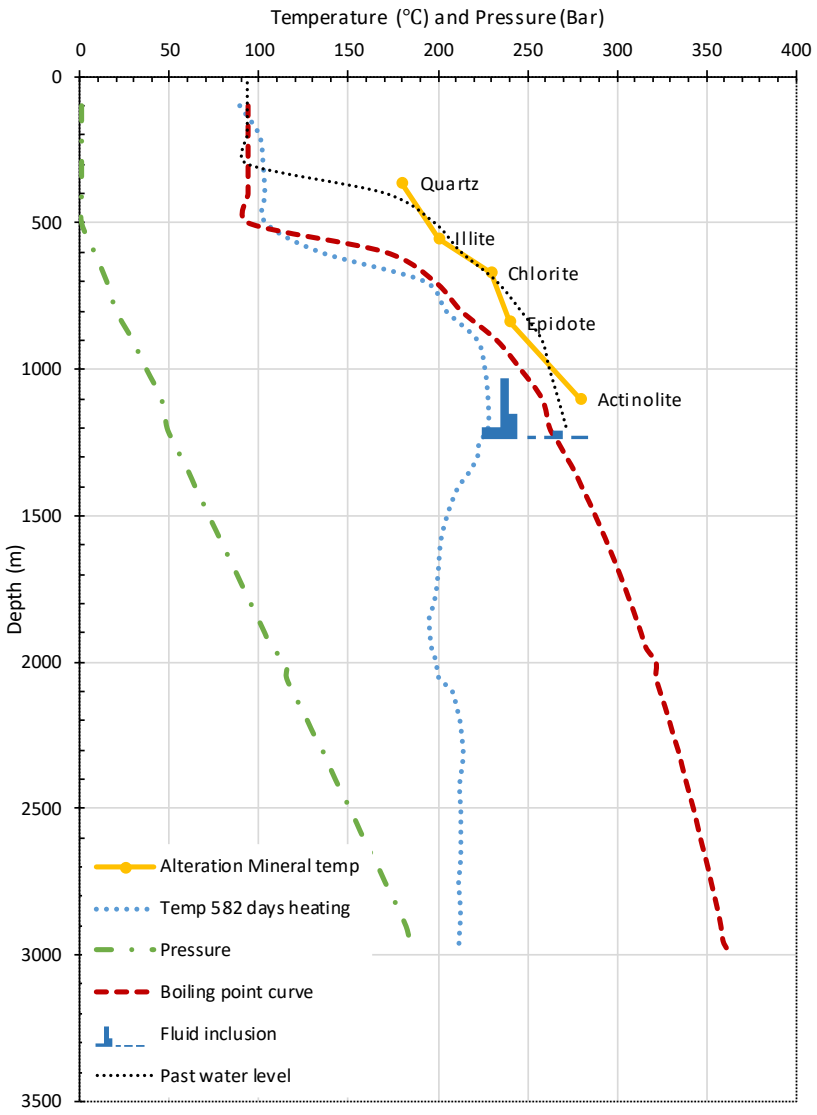

FIGURE 12: Comparison between alteration mineral temperature, boiling point curve, fluid inclusion and measured temperature

Temperatures reveal a significant difference between the past and the present temperatures of 30-50°C as indicated by the alteration minerals compared to the measured temperature today

which is observed at 500-1200 m depth in the well. At 1240 m depth the alteration minerals show temperatures of above 280°C. This temperature relates very well to the highest homogenisation temperatures of 280-285°C measured in fluid inclusions in calcite at 1238 m depth. A comparison of the boiling point curve and the alteration temperature curve shows that temperatures were higher (10-30°C) than the current boiling point temperature in the well. This difference indicates that the water table level which is currently at 500 m has been at 300 m based on the alteration minerals water table.

The measured temperature at 1240 m depth is 222°C. This temperature mimics the second regime of homogenisation temperatures in calcite which is 225-245°C at the same depth. These temperatures are both below the boiling point curve and can be interpreted to represent the present temperatures around this well. The measured temperature curve reveals even lower temperatures with depth. Between 1400 and 2050 m the temperature is 200°C while below 2050 m depth the temperature is 210°C.

4.8 Correlation with other wells in Olkaria Central and Olkaria Northeast field

Comparison of alteration temperature and measured temperature is useful for mapping outflow/upflow and inflow/downflow zones in a geothermal system. Areas with depressed temperatures are regarded as inflow/ downflow zones while areas with elevated temperatures are upflow zones. The three wells OW-202, OW-205 and OW-710 were used for alteration mineral correlation. Temperature isotherms were drawn from the first appearance of specific index minerals and the upper boundaries of the alteration zones were marked. This also represent the paleo-temperatures. First appearance of quartz, epidote and actinolite were interpreted to represent temperatures of 180, 240 and 280°C, respectively. The data was plotted in petrel and a W-E cross-section was drawn from OW-202 to OW-710 as shown in Figure 13.

The quartz and epidote isotherms are slightly dipping from OW-710 towards well OW-202. The quartz isotherm (180°C) lies at 1800 m a.s.l. in OW-710 and at 1400 m a.s.l. in well OW-202.

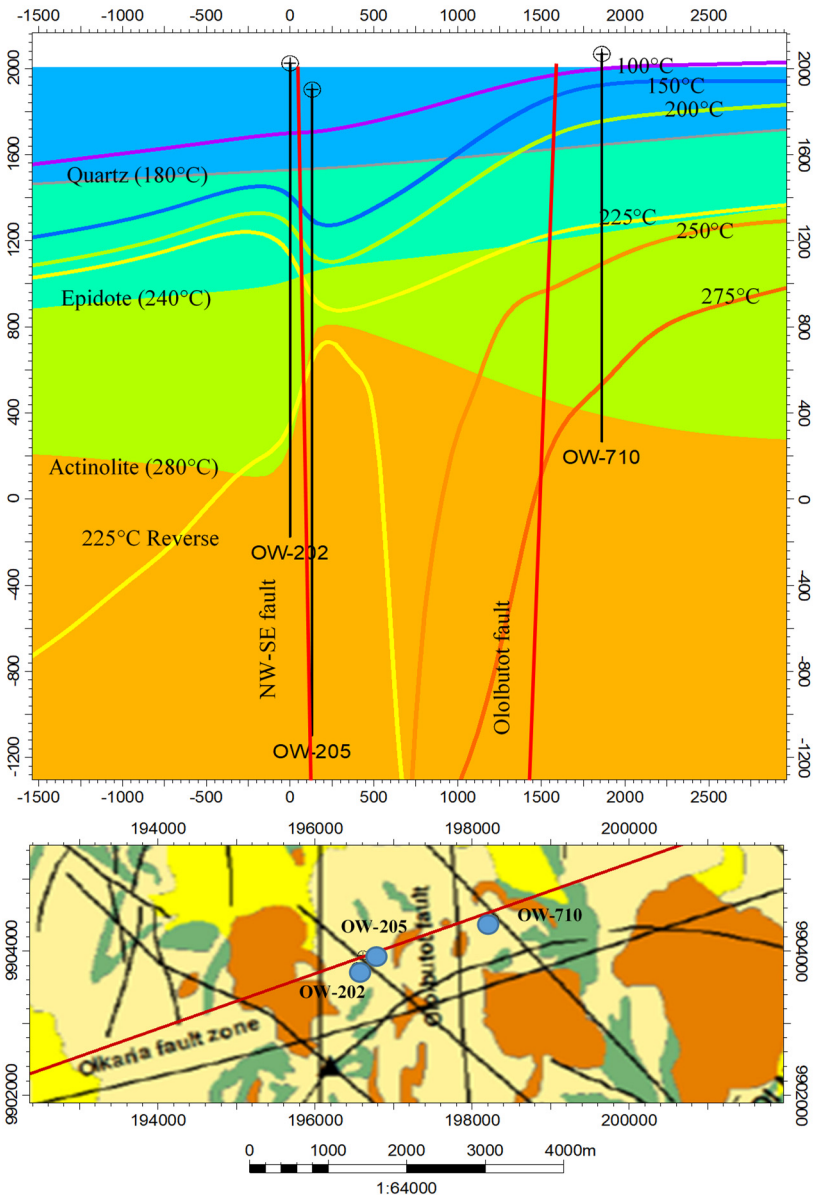

FIGURE 13: Correlation of alteration mineral zones between OW-202, OW-205 and OW-710

Temperatures of 240°C (epidote) seem to follow the same trend and reach from 1400 m a.s.l. in OW-710 to 900 m in OW-202. The actinolite isotherm shows noticeably elevated temperatures in well OW-205 at around 750 m a.s.l. but temperatures dip sharply towards OW-202 which could indicate some structural control of this zone. The sharp upward doming of the actinolite isotherm in OW-205 might indicate a possible up flow zone around this area.

The measured temperature seems to be in equilibrium with the alteration mineral temperatures around well OW-710 and formation temperatures are even higher than the alteration temperatures indicated by the quartz and epidote isotherms. This might indicate that well OW-710 is located near an upflow zone. Around well OW-202 and OW-205 temperature is almost in equilibrium with the temperature based on the alteration minerals from the surface and down to 800 m a.s.l. Below 700 m a.s.l., temperature reversal is observed, and measured temperatures decrease to less than 200°C. The 200°C isotherm lies within the supposed actinolite zone where paleo-temperatures were 280°C. This shows that temperature has decreased from 280°C (the formation temperature of actinolite) to below 200°C in both wells while the lowest temperatures are recorded in well OW-205. Reyes (1990) considered an index mineral occurring in an area where temperatures are ≥ 30°C below its stability temperature as relict that indicates cooling whereas minerals occurring in temperatures ≤ 30°C above its stability temperature indicate heating. Thus, the Ololbutot fault is a temperature divide with an upflow zone on the eastern side and an deep inflow zone on the western side.

5. DISCUSSION

5.1 Stratigraphy, faults and permeability

The well intersects eight rock units that were grouped two three major lithostratigraphic formations according to the Olkaria stratigraphy. The upper Olkaria volcanics occupies the top 700 m and comprises of pyroclastics, comendites, trachytes and minor basalts. Rocks in this zone are relatively fresh except for low-temperature zeolites and clays that are deposited in vesicles. Permeability in this section is mainly through pore spaces due to the unconsolidated nature of the pyroclastics layer and the fact that these rocks have not suffered great compression since no other layer overlies them.

The Olkaria basalts is a 360 m thick layer between the upper Olkaria volcanics and the plateau trachytes from 700-1060 m. It is mainly comprised of basalts with intercalations of tuff, rhyolites and trachytes. Due to the vesicular nature of the basalts, secondary minerals such as calcite precipitate and fill the vesicles and pores. This creates a steam capping layer, making this zone the cap rock in this well.

The plateau trachytes forms the bulk volume of the reservoir rock. It is about 1900 m thick and is dominated by trachytes with intercalations of basalt, rhyolites, tuff and sediments. Granitic and basaltic intrusions are intercepted between 2500 and 2800 m, occurring as thin layers of between 4 and 30 m.

A stratigraphic correlation of OW-205 with wells OW-202 and OW-710 indicate some fault related displacement (Figure 14). Well OW-205 is separated from OW-202 by a NW-SE fault in the west. This fault shows eastward displacement of around 60 m towards OW-205. The N-S Ololbutot fault is located between OW-205 and OW-710 and shows a westward displacement of around 650 m towards OW-205.

Subsurface permeability in this well is characterized by zones of lost circulation, fracturing and veining, high intensities of alteration as well as signs of oxidation. Minerals such as pyrite and calcite also indicate permeability. Major zones of lost circulation returns were encountered at 68-366, 754-826, 1014-1078 and 2176-2252 m, while minor loss zones and partial losses were encountered in most parts of the well, particularly between 400 and 1100 m.

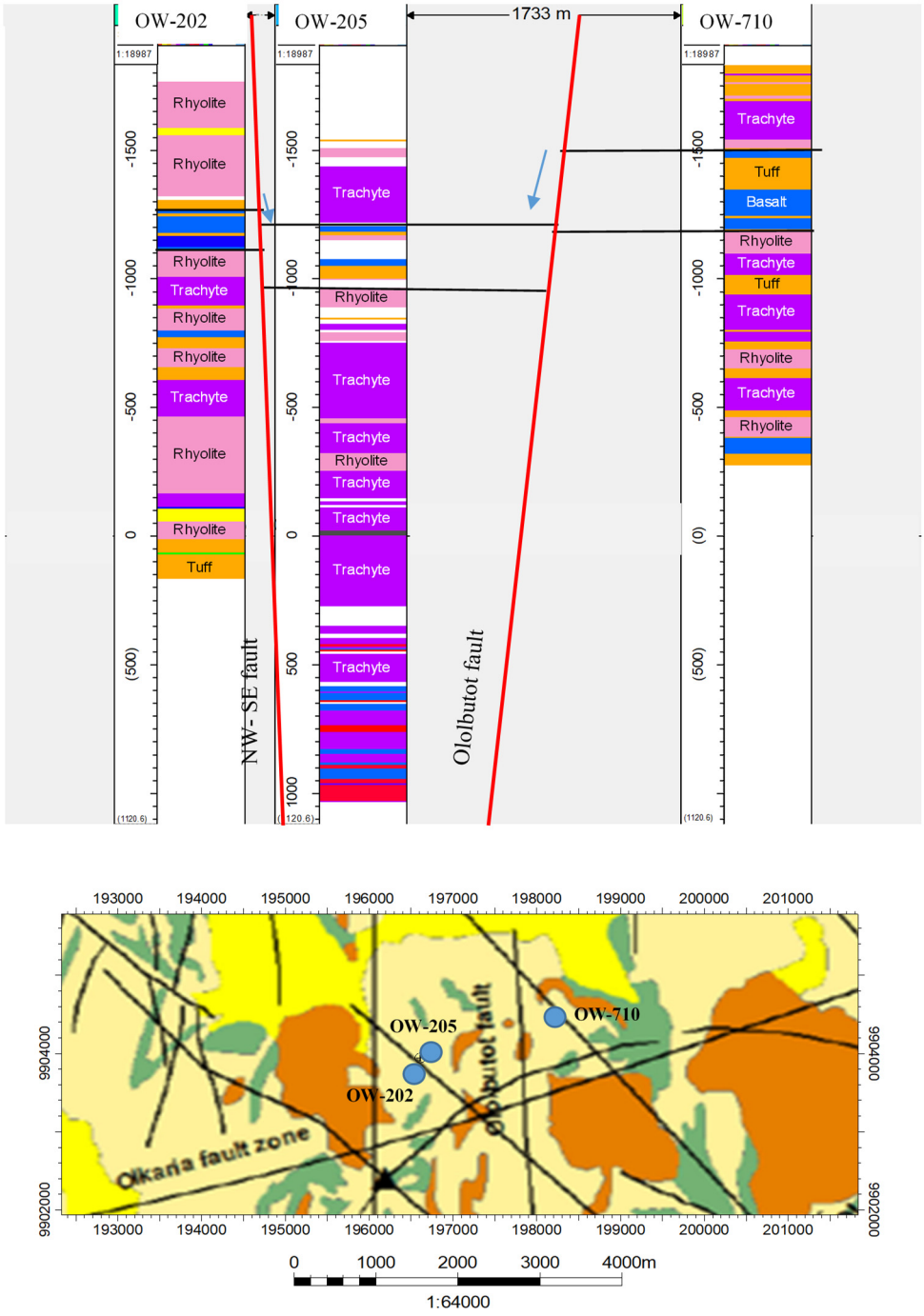

FIGURE 14: Stratigraphic correlation between wells OW-202, OW-205 and OW-710

Three major feed zones were identified at 754-978, 1182-1402 and 1784-2124 m. The first feed zone is a shallow aquifer occurring within the cap rock and it was cased-off. The other two are deep aquifers occurring within the reservoir rock. The feed zone at 1182-1402 m is characterised by high intensities of alteration, occurrence of high-temperature alteration minerals, vein filling, and abundance of calcite and pyrite. There is a decrease in temperature within this zone from 230°C at 1200 m to around 200°C at 1400 m. High intensities of oxidation are also observed in this zone. This feed point can be interpreted as a zone for inflow and mixing of cooler oxygenated fluids which is structurally controlled.

The feed zone between 1784-2124 m is both fractured with high intensities of high-temperature alteration and mineralogy. Abundant calcite, veining and multiple zones of lost circulation are observed.

This zone can also be interpreted as a channel for cooler fluids. Four minor feed zones are intercepted at 2174, 2470, 2666 and 2894 m. These zones are both related to intrusions, fracturing and vein-filling with high intensities of hydrothermal alteration but their permeability might be limited by the deposition of sphene, calcite, quartz, epidote and actinolite in the veins and vesicles. These zones are responsible for the convection heating of the fluids until they attain a stable temperature of about 210°C.

5.2 Temperature model

5.2.1 Processes controlling cooling

The presence of haematite and fluorite in the well could indicate conditions of cooling and oxidation related activities. The conditions controlling cooling in the well can be related to the same processes responsible for the formation of these minerals. Haematite, fluorite and sphene start to deposit in the well at around 800 m and persist to the bottom of the well though with varied intensities. For instance, haematite is observed in abundance between 1400-2000 m. It forms in environments where oxygen is readily available. The availability of oxygen would have been caused by low-temperature oxygenated fluids, probable meteoric waters, entering the well at this depth. The localised abundance of haematite at this depth indicates a lateral movement of cold meteoric fluids.

Fluorite forms as a younger mineral after epidote and actinolite in the well. Given that the presence of haematite points to oxygenated fluids, fluorite is likely to have formed when these cold fluids, which are Ca-rich, mix with the brine. Another possibility is the mixing of two brines of different chemical composition. Well OW-205 is separated from OW-202 by a NW-SE fault in the west and from well OW-710 by the N-S Ololbutot fault in the east. The NW-SE east dipping faults are considered the main faults and provide deep recharge into the system. The rejuvenated N-S faults, e.g. the Ololbutot fault control the shallow ground water movement and are responsible for temperature inversions in OW-201 (Omenda, 1998). Bodvarsson and Pruess (1987) deduced that recharge from the Olkaria west and Olkaria northeast fields are mixed around well 201 through the Olkaria fracture and Ololbutot fault, respectively. Thus, fluorite formation due to brine mixing is also a possibility given that the fluids in the area around well OW-205 are of mixed composition.

The presence of sphene is distinct in the well and its occurrence is characterised by zonation. It occurs in the upper part of the well from 900-1200 m and later in abundance from 2000 m to the bottom of the well while it occurs only in insignificant concentration between 1200- 2000 m where the temperature reversal occurs. Occurrence of sphene is commonly related to replacement of FeTi-oxides but the zonation in OW-205 could indicate that the abundance of sphene is also affected by mixing of cooler fluids, though this is something that needs to be studied further.

5.2.2 Structural control of the temperature model

Both past and present temperatures were studied in the well. Temperature correlations between alteration mineral temperatures and measured temperatures in wells OW-202, OW-205 and OW-710 revealed near equilibrium conditions at shallow depths down to around 700 m when temperature isotherms around OW-205 start to deepen compared to the other wells. This near surface equilibrium confirms that the cooling does not occur vertical from above but rather that inflow of colder fluids is flowing more lateral at this depth. It can be interpreted that cold fluids form a deep inflow along the N-S Olobutot fault or deep cold inflow from rift escarpment along NW-SE faults into the Olkaria Central Field.

The localised upflow zone around OW-205, indicated by the paleo-temperatures for actinolite, can be associated with the NW-SE fault. This NW-SE fault is regarded to be one of the oldest faults in the rift. Temperature comparison between measured temperatures, alteration mineral temperature, and homogenisation temperature at 1238 m revealed a temperature decrease from 285 to 225°C. The

alteration mineral temperature is higher (285°C) than the measured temperature (225°C) at this depth. Fluid inclusion recorded a temperature range of 225-285°C and a stationary temperature of 235-245°C indicating that temperatures have been at this interval for most of the time. The two temperature regimes deduced from fluid inclusion further confirm the fact that the paleo temperatures were higher (285°C) compared to the present temperature of 225°C, thus making the previous localised upflow zone in OW-205 to be a flow path for cooler fluids in current time. It can be interpreted that the area east of this fault was once an upflow zone and cooler conditions occurred later, maybe after the rejuvenation of the N-S faults. This change is likely to have introduced a new flow path and channelled cold fluids toward this zone of prior upflow around well OW-205.

Temperatures east of Ololbutot around OW-710 indicate that this part of the field is heating up as measured temperatures in this region are higher than the alteration temperatures. This recent event is also associated with the rejuvenation of the Ololbutot fault. This fault controls an upflow zone on the eastern side and an inflow zone on the western side.

Figure 15 represents the current model of temperatures around well OW-205 and the flow of cooler fluids along the Ololbutot and the NW-SE faults.

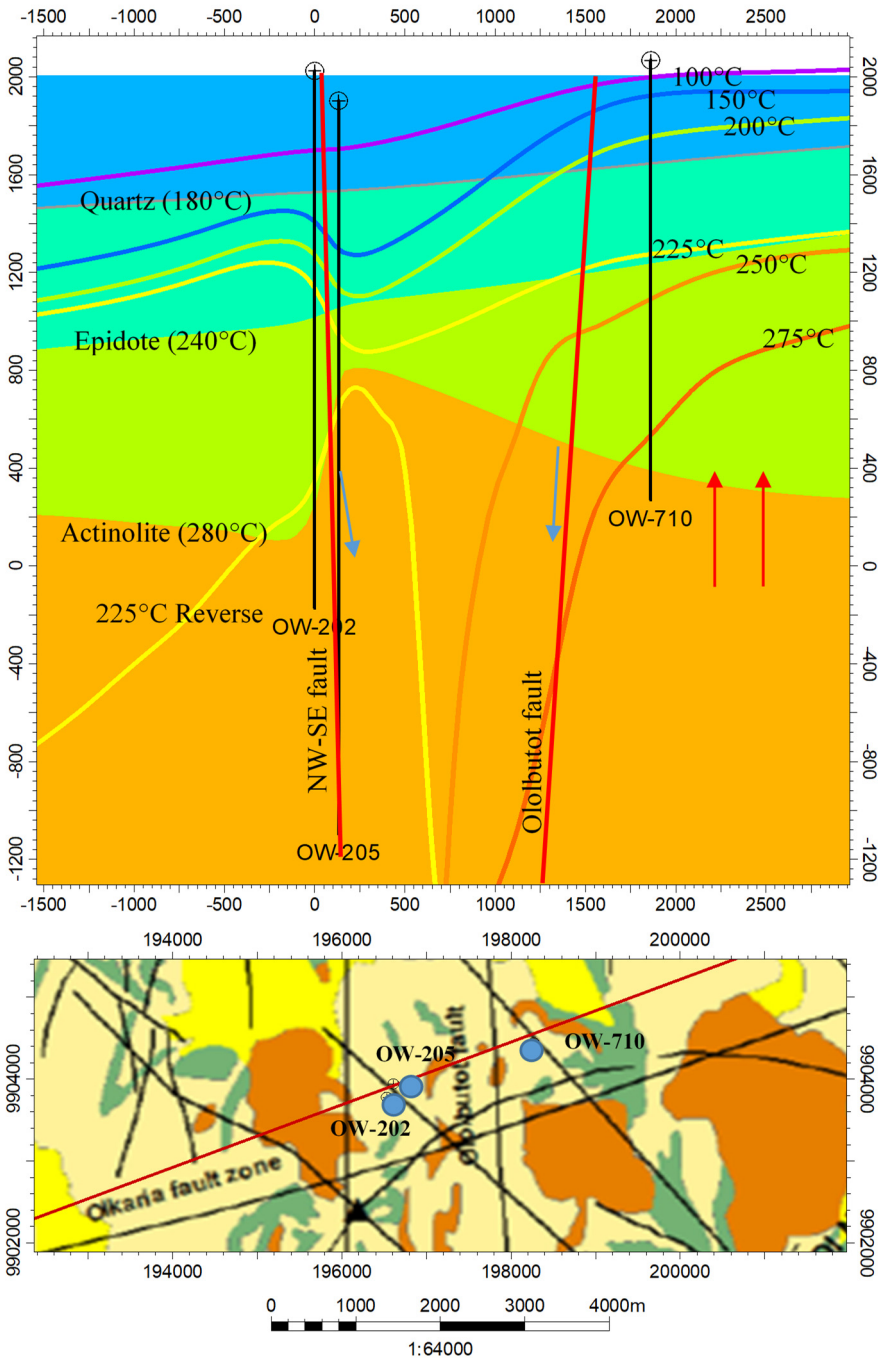

FIGURE 15: Temperature and fluid flow model for the area around OW-205 (red arrows indicate upflow along Ololbutot fault, blue arrows indicate vertical down flow)

6. CONCLUSION AND RECOMMENDATIONS

High-temperature minerals were observed in the well including epidote and actinolite indicating paleo-temperatures of 240 and 280°C at 842 and 1100 m, respectively. The well is fed by two major feed zones controlled by the Ololbutot fault in the east and the NW-SE fault west of the well. These zones provide lateral flow and are responsible for the incursion of cooler fluids and subsequent temperature reversals at 1400-2100 m. Comparison of temperature patterns indicate that the past and present temperatures are not in equilibrium. This points to the conclusion that the area in vicinity of well OW-205 was in the past a localized upflow zone but it is presently a recharge zone for cool fluids.

The initial expectation for this well was to provide steam for Olkaria VII power plant and to open up the Olkaria Central Field. This was based on the potential of OW-202 which was confirmed to be better (1.4 MWe) than other wells in the Olkaria Central Field, e.g. wells OW-201 and OW-204 which failed to discharge. Being directly opposite of OW-202 and separated by the NW-SE fault, this well was expected to have the same potential or even higher production rates than well OW-202. It was located northeast of OW-202 with the aim to target higher temperatures on the eastern side of the fault but temperatures turned were not higher. The cooling along this fault was not expected since the NW-SE faults are known to control both shallow and deep upflow zones.

Because of the relatively low temperatures, it will likely be difficult to get well OW-205 to discharge. And even if there is a way to discharge the well, the temperatures are still very low that it would only be suitable for Ormat or a well head unit designed specifically for this well. Therefore, it is only practical to convert the well into an injection well since it is situated in a natural flow path of recharge.

Fluid inclusion analysis was based on only one calcite crystal, thus more analysis from several crystals is required to get a more confident picture of the temperature distribution. Fluorite is a young alteration mineral associated with the temperature reversal in the well, therefore fluid inclusion analyses of inclusions in fluorite is recommended to confirm the temperatures at which it has precipitated and to outline the processes controlling cooling; whether it is the heating of cold ground water or cooling and mixing of hot brine. Similarly, a comparison of the groundwater chemistry and the reservoir fluid is necessary to determine the processes governing the cooling conditions in the area.

ACKNOWLEDGEMENTS

I take this opportunity to thank the Government of Iceland and the United Nations University Geothermal Training Programme (UNU-GTP) for the award of the fellowship and my employer Kenya Electricity Generating Company (KenGen) for granting me the approval to attend the course. Special thanks to the Director of UNU-GTP, Mr. Lúdvík S. Georgsson, deputy director, Mr. Ingimar G. Haraldsson, Mr. Markús A.G. Wilde, Málfrídur Ómarsdóttir and Dr. Vigdís Hardardóttir for their availability in coordination and facilitation throughout the study period.

Am also indebted to my supervisors Ms. Anette K. Mortensen together with Mrs. Helga Margrét Helgadóttir and Mr. Tobias Weisenberger for their dedicated guidance and technical support throughout the project. Not to forget Mr. Sigurdur Sveinn Jónsson for his assistance in XRD analysis and interpretation, Dr. Hjalti Franzson for the field trips and all the ÍSOR staff, for their contributions making this training success. Special thanks go to my fellow geologists and the UNU 2019 six month's fellows for the support we provided for each other that really created a productive and homely environment.

Special thanks go to my beloved parents, my husband Mwijaka and my children Cynthiacate, Josephine and Maxwell for their interminable love, encouragement and support while enduring my absence during the six months period.

Above all, I thank the Almighty God for his grace and mercy.

REFERENCES

Bailey, D, K., 1974: Melting in the deep crust. In: Sorensen, H. (ed.). *The alkaline rocks.* Wiley, London, 436-442.

Baker, B.H., Mohr, P.A., and Williams, L.A.J., 1972: Geology of the Eastern Rift System of Africa. *Contrib. GSA Special Papers, 136*, 1-68.

Bhogal P., and Skinner M., 1971: *Magnetic surveys and interpretation in the Olkaria geothermal area.* Report prepared for the Kenya Power Company, Ltd., 15 pp.

Bodvarsson, G.S., and Pruess, K., 1987: *Numerical simulation studies of the Olkaria geothermal field.* Kenya Power Company Ltd., internal report.

Browne, P.R.L., 1984: Subsurface stratigraphy and hydrothermal alteration of Eastern section of the Olkaria geothermal field, Kenya. *Proceedings of the 6th New Zealand Geothermal Workshop, Geothermal Institute, Auckland, NZ,* 33-41.

Chorowicz, J., Collet, B., Bonavia, F., Mohr, P., Parrot, J.F., and Korme, T., 1998: The Tana basin, Ethiopia: Intra-plateau uplift, rifting and subsidence. *Tectonophysics, 295*, 351–367.

Clarke, M.C.G., Woodhall, D.G., Allen, D., and Darling G., 1990: *Geological, volcanological and hydrogeological controls on the occurrence of geothermal activity in the area surrounding Lake Naivasha, Kenya, with coloured 1:100 000 geological maps.* Ministry of Energy, Nairobi, 138 pp.

Fritz, H., Abdelsalam, M., Ali, K.A., Bingen, B., Collins, A.S., Fowler, A.R., Ghebreab, W., Hauzenberger, C.A., Johnson, P.R., Kusky, T.M., Macey, P., Muhongo, S., Stern, R.J., Viola, G., 2013: Orogen styles in the East African Orogen: A review of the Neoproterozoic to Cambrian tectonic evolution. *J. African Earth Sciences, 86*, 65–106.

Guilbert, J.M. and Park, C.P. 1986. *The geology of ore deposits*. W.H. Freeman, NY, 985 pp.

Hara, J., and Tsuchiya, N., 2004: *Coupled T (thermal) - H (hydrological) - C (chemical) process of geothermal alteration, based on experimental and kinetic considerations*. Elsevier, Geo-Engineering Book Series, 2*,* 6 pp.

Hoffman, C., Courtillot, V., Feraud, G., Rochette, P., Yirgu, G., Ketefo, E., and Pik, R., 1997: Timing of the Ethiopian flood basalt event: implications for plume birth and global change. *Nature, 389*, 838–841.

Hughes, G.W., Varols, O., and Beydoun, Z.R., 1991: Evidence for Middle Oligocene rifting of the Gulf of Aden and for Late Oligocene rifting of the Southern Red Sea. *Marine and Petroleum Geology, 8,* 354-358.

Kampunzu, A.B., Bonhomme, M.G., and Kanika, M., 1998. Geochronology of volcanic rocks and evolution of the Cenozoic Western Branch of the East African Rift System. *J. African Earth Sci., 26,* 441–461.

Kamunya, K.M., 2014: *Update of the Olkaria geochemical conceptual model*. KenGen, Kenya, internal report.

Kamunya, K.M., 2018: *δD and δ18O systematics in geothermal fluids, Olkaria geothermal system, Kenya.* University of Iceland, Reykjavík, MSc thesis, UNU-GTP, Iceland, report 4, 41 pp.

Karingithi, C.W., 2000: Geochemical characteristics of the Greater Olkaria geothermal field, Kenya. Report 9 in: *Geothermal training in Iceland 2000*, UNU-GTP, Iceland, 165-188.

Karingithi, C.W., Arnórsson, S., and Grönvold, K., 2010: Processes controlling aquifer fluid compositions in the Olkaria geothermal system, Kenya. *J. Volc. and Geothermal Res., 196,* 57-76.

KenGen, 2017: *Geothermal resource map*. KenGen, internal report.

Kerr, P.F., 1959: *Optical mineralogy* (3rd edition). McGraw-Hill Book Company, NY, 442 pp.

Kristmannsdóttir, H., 1979: Alteration of basaltic rocks by hydrothermal activity at 100-300°C. In: Mortland, M.M., and Farmer, V.C. (editors), International Clay Conference 1978. Elsevier Scientific Publishing Co., Amsterdam, 359-367.

Lagat, J.L., 1998: *Borehole geology of well OW-801, Olkaria South East field*. KenGen, Kenya, internal report, 12 pp.

Lagat, J.K., 2004: *Geology, hydrothermal alteration and fluid inclusion studies of the Olkaria Domes geothermal field, Kenya.* University of Iceland, MSc thesis, UNU-GTP, Iceland, report 1, 79 pp.

Leach, T.M., and Muchemi G.G., 1987: Geology and hydrothermal alteration of the North and West exploration wells in the Olkaria geothermal field, Kenya. *Proceedings of the 9th New Zealand Geothermal Workshop, Auckland, NZ,* 187-192.

Macdonald, R., 2002: Magmatism of the Kenya Rift Valley: a review. *Earth and Environmental Transactions of the Royal Society of Edinburgh, 93-3*, 239-253.

MacDonald, R., and Scaillet, B., 2006: The central Kenya peralkaline province: insights into the evolution of peralkaline salic magmas. *Lithos, 91*, 59-73.

Marshall, A.S., Macdonald, R., Rogers, N.W., Fitton, J.G., Tindle, A.G., Nejbert, K., and Hinton, R.W., 2009: Fractionation of peralkaline silicic magmas: the greater Olkaria volcanic complex, Kenya Rift Valley. *J. Petrology, 50-2,* 323–359.

Munyiri, S.K., 2016: *Structural mapping of Olkaria Domes geothermal field using geochemical soil gas surveys, remote sensing and GIS.* University of Iceland, MSc thesis, UNU-GTP, Iceland, report 5, 73 pp.

Mutua, B.W., 2014: An overview of geochemical characteristics of Olkaria geothermal field, Kenya. *Proceedings of the 5th African Rift Geothermal Conference – ARGeo 5, Arusha, Tanzania,*8 pp.

Ndombi, J.M., 1981: The structure of the shallow crust beneath the Olkaria geothermal field, Kenya, deduced from gravity studies. *J. Volcanology and Geothermal Research, 9*, 237-251.

Nicholson, K., 1993: *Geothermal fluids: chemistry and exploration techniques*. Springer-Verlag, Berlin, 268 pp.

Odongo, M.E.O., 1993: A geological review of Olkaria geothermal reservoir based on structure. *Proceedings of the 15th New Zealand Geothermal Workshop, Auckland, NZ, 169-173.*

Ofwona, C., Omenda, P., Mariita, N., Wambugu, J., Mwawongo, G., and Kubo, B., 2006: *Surface geothermal exploration of Korosi and Chepchuk prospects.* KenGen, Kenya, internal report, 44 pp.

Omenda, P.A., 1998: The geology and structural controls of the Olkaria geothermal system, Kenya. *Elsevier Science Ltd., 27-1*, 55-74.

Omenda, P.A., 2000: Anatectic origin for comendite in Olkaria geothermal field, Kenya Rift; Geochemical evidence for syenitic protholith. *African J. Science and Technology, Science and Engineering Series, 1*, 39-47.

Opondo, K., 2015: Carbonate scale formed in well OW-202 in Olkaria Central field, Kenya. *Proceedings of the World Geothermal Congress, Melbourne, Australia*, 10 pp.

Raith, M.M., Raase, P., and Reinhardt, J., 2012: *Guide to thin section microscopy* (2nd ed.). e-Book ISBN 978-3-00-037671-9 (PDF) 127 pp, website: *www.minsocam.org/msa/openaccess_publications/Thin_Sctn_Mcrscpy_2_prnt_eng.pdf*

Randive, K., Hari, K.R., Dora, M.L., Malpe, D.B., and Bhondwe, A., 2014: Study of fluid inclusions: methods, techniques and applications. *Gondwana Geological Magazine, 291*, 19-28.

Reed, M.H., 1997: Hydrothermal alteration and its relationship to ore fluid composition. In: Barnes, H.L. (ed.), *Geochemistry of hydrothermal ore deposits* (3rd ed.). John Wiley & Sons, NY, 517-611.

Reyes, A.G., 1990: Petrology of Philippine geothermal systems and the application of alteration mineralogy to their assessment. *J. Volc. Geoth. Res., 43,* 279-309.

Richardson, C.K., and Holland, H.D., 1979: Fluorite deposition in hydrothermal systems. *Geochim. Cosmochim. Acta, 43,* 1327-1335.

Rop, E., 2013: Interpretation of recent temperature and pressure data and updated conceptual model of the Greater Olkaria geothermal system, Kenya. Report 32 in: *Geothermal training in Iceland*. UNU-GTP, Iceland, 769-806.

Rop, E., Fujii, H., and Jalilinasrabady, S., 2018: An updated numerical model of the Greater Olkaria geothermal system, Kenya. *Proceedings of the 43rd Workshop on Geothermal Reservoir Engineering Stanford University, Stanford, CA,* 85-97.

Saemundsson, K., 2010: East African Rift System – an overview. *Presented at Short Course V on Exploration for Geothermal Resources, organised by UNU-GPT, GDC and KenGen, at Lake Bogoria and Lake Naivasha, Kenya,* 8 pp.

Saitet, D., and Kwambai, C., 2015: Wellhead generating plants: KenGen experience. *Proceedings of the World Geothermal Congress 2015, Melbourne, Australia*, 6 pp.

Salvi, S., and Williams-Jones, A.E., 2006: Alteration, HFSE mineralisation and hydrocarbon formation in peralkaline igneous systems: Insights from the Strange Lake Pluton, Canada. *Lithos, 91,* 19–34.

Schwartz, G.M., 1950: Problems in the relation of ore deposits to hydrothermal alteration. *Q.J. Colorado Sch. Mines, 45,* 196-208.

Simiyu, S.M., and Keller, G.R., 1997: Integrated geophysical analysis of the East African plateau from gravity anomalies and recent seismic studies. *Tectonophysics, 278,* 291–314.

Simmons, S.F. and Christenson, B.W., 1994: Origin of calcite in a boiling geothermal system. *Am. Jour. Sci.*, *294,* 361-400.

Wanjohi, A.W., 2014: Geophysical survey of a high-temperature field, Olkaria. *Presented at "Short Course IX on Exploration for Geothermal Resources", organized by UNU-GTP, GDC and KenGen, at Lake Bogoria and Lake Naivasha, Kenya*, 30 pp.

West-JEC, 2009: *The Olkaria optimization study (phase ii), final reservoir analysis report*. KenGen, Kenya, West Japan Engineering Consultants, Inc., report, 301 pp.

Yirgu, G., 2009: An outline of the East African Rift volcanism. *Advanced Workshop on Evaluating, Monitoring and Communicating Volcanic and Seismic Hazards in East Africa, Addis Ababa University Ethiopia,* 19 pp.

APPENDIX I: XRD results and examples of interpretation for kaolinite, illite and chlorite

TABLE 1: XRD results and interpretation

No.	Depth (m)	First order{d(001)}(Å)			Second order{d(002)}(Å)			Alteration mineral
		U	G	H	U	G	H	
1	512-514							none
2	552-554	10.1	10.1	10.1				Illite
		7.1	7.1	7.1				Kaolinite
3	636-638	10.1	10.1	10.1				Illite
		7.1	7.1	7.1				Kaolinite
4	732-734	14.7	14.7	14.7	7.2	7.2	0	Unstable chlorite
		10.3	10.3	10.3				Illite
5	854-856	14.6	14.6	14.6	7.2	7.2	0	Unstable chlorite
		10.2	10.2	10.2				Illite
6	996-998	14.7	14.7	14.7	7.2	7.2	0	Unstable chlorite
		10.2	10.2	10.2				Illite
7	1080-1082	14.7	14.7	14.7	7.2	7.2	0	Unstable chlorite
		10.2	10.2	10.2				Illite
8	1100-1102	14.6	14.6	14.6	7.2	7.2	0	Unstable chlorite
		10.3	10.3	10.3				Illite
9	1194-1196	14.6	14.6	14.6	7.2	7.2	0	Unstable chlorite
		10.3	10.3	10.3				Illite
10	1248-1250	14.6	14.6	14.6	7.2	7.2	7.2	Stable chlorite
		10.3	10.3	10.3				Illite
11	1416-1420	14.5	14.5	14.5	7.2	7.2	0	Unstable chlorite
		10.3	10.3	10.3				Illite
12	1886-1888	14.5	14.5	14.5	7.2	7.2	0	Unstable chlorite
		10.3	10.3	10.3				Illite
13	2276-2280							None
14	2462-2466	14.5	14.5	14.5	7.2	7.2	0	Unstable chlorite
		10.2	10.2	10.2				Illite
15	2706-2708	10.4	10.4	10.4				Illite

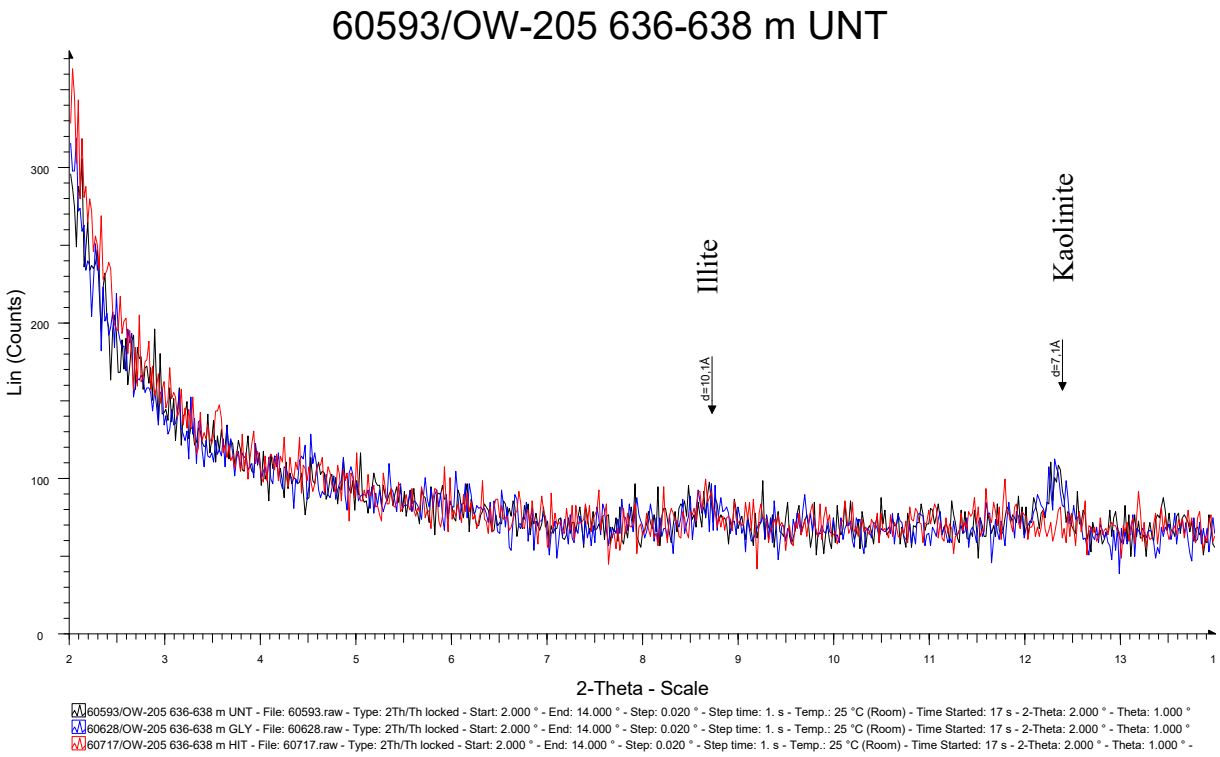

FIGURE 1: XRD analysis showing small illite and kaolinite peaks

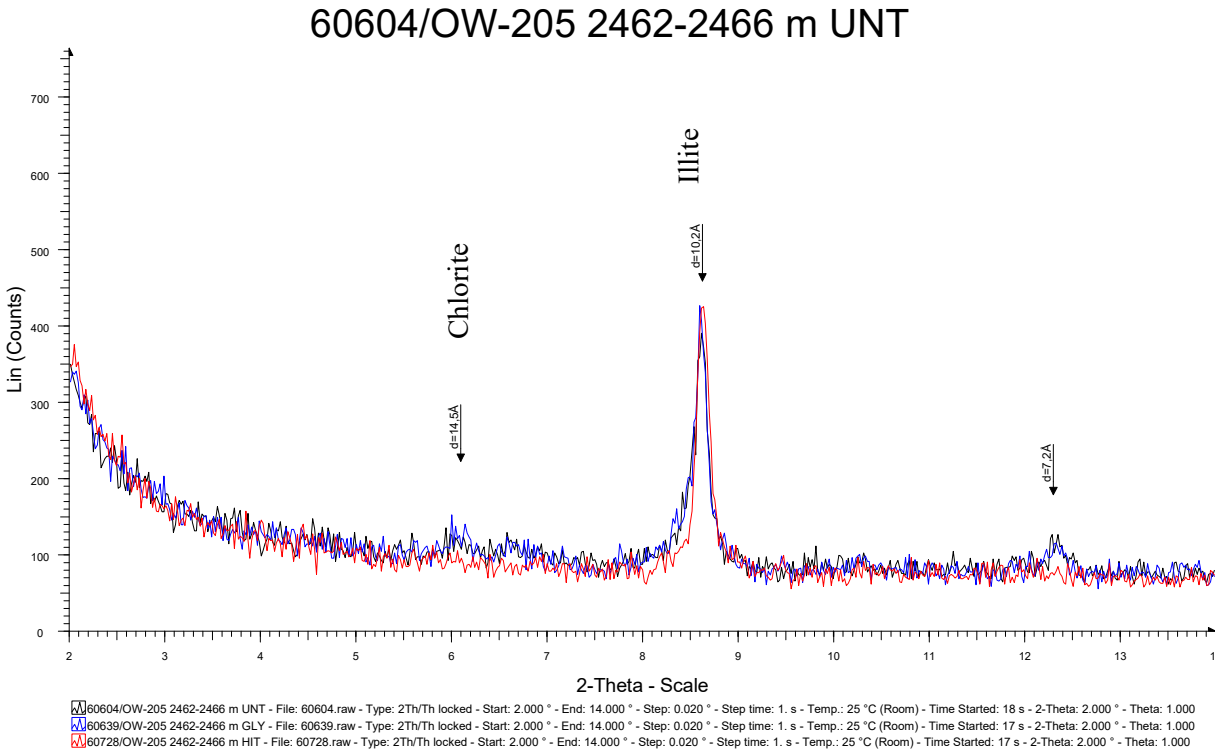

FIGURE 2: XRD analysis showing distinct illite peak and small chlorite peaks